

Adding detritus to a nutrient–phytoplankton–zooplankton model: a dynamical-systems approach

ANDREW M. EDWARDS

BIOLOGICAL OCEANOGRAPHY SECTION, BEDFORD INSTITUTE OF OCEANOGRAPHY, DARTMOUTH, NOVA SCOTIA, B2Y 4A2, CANADA

The dynamics of two plankton population models are investigated to examine sensitivities to model complexity and to parameter values. The models simulate concentrations of nutrients, phytoplankton, zooplankton and detritus in the oceanic mixed layer. In Model 1, zooplankton can graze only upon phytoplankton, whereas in Model 2 they can graze upon phytoplankton and detritus. Both feeding strategies are employed by zooplankton in the ocean, and both are features of models in the literature. Each model here consists of four coupled ordinary differential equations, and can exhibit unforced oscillations (limit cycles) of the four concentrations. By constructing diagrams that show how steady states and oscillations persist as each parameter is varied, a general picture of the dynamics of each model is built up. The addition of the detritus pool to an earlier nutrient–phytoplankton–zooplankton model appears to have little influence on the dynamics when the zooplankton cannot graze upon the detritus (Model 1), but if the zooplankton can graze upon the detritus (Model 2), then the dynamics are affected in a significant way. These results, obtained using the theory of dynamical systems, enhance our knowledge of the factors governing the dynamics of plankton population models.

INTRODUCTION

In addition to the practical difficulties of data collection and interpretation, oceanographers are faced with conceptual challenges when constructing models of the plankton ecosystem. One such challenge involves deciding how many components of the ecosystem should be explicitly included in a model. Hilborn and Mangel (Hilborn and Mangel, 1997) stated that, for ecological models in general, ‘Perhaps the most difficult decision in model building is “How complex should the model be?”’ (p. 36). The answer will depend upon the purpose of the model and on the available data. Here we are interested in understanding how such choices will influence the dynamics of the model.

Of particular relevance to this study is the fact that some models do not explicitly contain a detritus compartment [e.g. (Steele and Henderson, 1981, 1992, 1993; Evans and Parslow, 1985; Franks *et al.*, 1986)] whereas others do [e.g. (Hofmann and Ambler, 1988; Fasham, 1993, 1995; Oschlies and Garçon, 1998, 1999; Fennel *et al.*, 2001)]. Here, we investigate how the addition of a detritus compartment to a simple nutrient–phytoplankton–zooplankton (*NPZ*) model changes the

dynamics of the original *NPZ* model. This is of interest because results derived from simple models, such as by Steele and Henderson (Steele and Henderson, 1992), are often used to help guide the construction and implementation of larger models, such as the seven-component Fasham model (Fasham, 1993). But the addition of the extra components that transform an *NPZ* model into a seven-component model may change the dynamics so profoundly that conclusions concerning the *NPZ* model no longer apply.

Detritus consists of faecal pellets of zooplankton, plus dead phytoplankton and zooplankton (Fasham *et al.*, 1990). Attached bacteria can break down the detritus into utilizable nutrient, a process known as remineralization. Detrital particles can aggregate together and sink out of the mixed layer, a mechanism that plays an important part in exporting carbon to the deep ocean. Furthermore, detritus can be grazed upon by zooplankton (Paffenhöfer and Strickland, 1970; Paffenhöfer and Knowles, 1979). This depends upon the species composition of the zooplankton, and is included in some models that incorporate zooplankton and detritus (Fasham *et al.*, 1990; Fasham, 1993; Popova *et al.*, 1997), but excluded from others [Hood and Olson’s model in Davis and Steele

(Davis and Steele, 1994); (Fasham, 1995; Denman and Peña, 1999)].

We investigate the dynamics of two plankton models, each explicitly modelling mixed-layer concentrations of nutrient, phytoplankton, zooplankton and detritus (D). The aim here is to understand the dynamics of models, rather than to attempt to simulate any particular data set. The models are extensions of the NPZ model studied by Edwards and Brindley (Edwards and Brindley, 1996), which was the model of Steele and Henderson (Steele and Henderson, 1981) modified in the manner of Steele and Henderson (Steele and Henderson, 1993). The addition of the detrital component to yield an $NPZD$ model represents a major structural difference from the original NPZ model; here we consider two $NPZD$ models. In Model 1, we do not allow zooplankton to graze on detritus, whereas we do include such grazing in Model 2. This is so that we increase the complexity of the models one step at a time, making it clear which particular amendment brings about any change in dynamical behaviour.

Previous work on the nature of steady states in NPZ and $NPZD$ models without physical forcing has helped modellers to understand the dynamics that occur when these biological models are then coupled to physical models (Flierl and Davis, 1993; Olson and Hood, 1994; Franks and Walstad, 1997). In particular, Edwards *et al.* (Edwards *et al.*, 2000a,b) (not the current author) have investigated the behaviour of another NPZ model (Franks *et al.*, 1986) when it is coupled with a vertical mixing model and a coastal upwelling model. The authors extensively utilized the detailed characterization by Busenberg *et al.* of the steady states and oscillations of the original NPZ model (Busenberg *et al.*, 1990). Furthermore, Scheffer *et al.* examined a PZ model, showing how a detailed characterization of bifurcations (defined here later) can explain the abrupt changes in population dynamics often observed in lakes (Scheffer *et al.*, 2000).

Oscillations of variables have attracted much interest [e.g. (Popova *et al.*, 1997; Caswell and Neubert, 1998)], prompted by the work of Steele and Henderson, who found oscillations to occur only when zooplankton mortality was modelled using a linear function of the zooplankton, and not a quadratic function (Steele and Henderson, 1992). It was then shown (Edwards and Brindley, 1996, 1999) that oscillations can, in fact, occur when the quadratic function is used, but indeed do appear to be more common with the linear function. Ryabchenko *et al.* (Ryabchenko *et al.*, 1997) and Edwards and Yool (Edwards and Yool, 2000) have examined similar oscillations that occur in the Fasham (Fasham, 1993) model under summertime conditions, when the physical forcing is minimal.

Moreover, such oscillations have been observed in the real ocean. For example, short-term oscillations of chloro-

phyll values are revealed in data from Ocean Weather Station I in the north-east Atlantic Ocean (Williams, 1988). Ryabchenko *et al.* (Ryabchenko *et al.*, 1997) noted that such oscillations may be due to factors other than simple predator–prey cycles, but that, nevertheless, these intriguing features of models are of interest and warrant investigation. Furthermore, oscillations have been reported in a variety of freshwater plankton populations (McCauley and Murdoch, 1987). Because of similarities with the dynamics of laboratory populations, from which external physical forcing is excluded, it was concluded that the oscillations were a result of ecological interactions. The oscillations found in our models are due to ecological interactions, since no physical forcing is included.

We examine steady states and oscillations of the four variables in our $NPZD$ models. First, we formulate Model 1, and (in the Appendix) summarize what can be deduced analytically from the equations, using a ‘paper-and-pencil’ approach, without using particular numerical values for the parameters. Two time series are then shown; the first demonstrates the system settling down to a steady state (whereby all four variables reach constant values), and the second demonstrates oscillations of the variables. This leads us to construct bifurcation diagrams showing how the oscillations persist as each of the parameters of the model is independently varied. The diagrams show the bifurcational behaviour of the original NPZ system [determined by Edwards and Brindley (Edwards and Brindley, 1996)] to be remarkably preserved in the $NPZD$ system, and can be thought of as giving a general picture of the behaviour of the model across realistic ranges of parameters. Next we discuss how the period of the oscillations changes as each of the parameters is varied. The results for Model 1 show that, by itself, adding the detritus compartment to the NPZ model has little effect upon the qualitative dynamics of N , P and Z .

Then we formulate Model 2, which incorporates zooplankton feeding on detritus, and follow the same investigational approach as for Model 1. We find that the oscillations still occur, but they have a longer period and occur across smaller parameter ranges than for Model 1. So, including such feeding by zooplankton seems to have more effect upon the dynamics of the models than merely adding the new detritus compartment to the original NPZ model. We end by discussing the results in relation to previous plankton modelling work.

Comprehensive mathematical details of bifurcations are kept to a minimum in this paper [but are given by Edwards (Edwards, 1997)]. Here we focus upon the general nature of the results, occasionally elaborating on the details in order to explain the features of diagrams fully. Further aspects concerning the theory of dynamical systems, which encompasses bifurcations, can be found

elsewhere [e.g. the books by (Thompson and Stewart, 1986; Murray, 1989; Wiggins, 1990; Glendinning, 1994; Kuznetsov, 1995)]. For brevity, hereafter we use the following abbreviations for papers: EB96 (Edwards and Brindley, 1996); SH81, SH92 and SH93 (Steele and Henderson, 1981, 1992, 1993).

FORMULATION OF MODEL 1

Figure 1 shows the structure of Model 1, with arrows indicating flows of matter between the four modelled compartments: nutrient (N), phytoplankton (P), zooplankton (Z) and detritus (D). The arrow not starting at any compartment indicates the input to the system (nutrients entering from below the mixed layer), and arrows not ending at a compartment represent losses from the modelled system. We assume a spatially homogeneous mixed layer, with the changes in N , P , Z and D given by:

$$\frac{dN}{dt} = - \text{uptake} + Z \text{ excretion} + Z \text{ predation excretion} + D \text{ remineralization} + \text{mixing}$$

$$\frac{dP}{dt} = \text{uptake} - \text{respiration} - \text{grazing by } Z - \text{sinking} - \text{mixing}$$

$$\frac{dZ}{dt} = \text{growth} - \text{higher predation}$$

$$\frac{dD}{dt} = P \text{ respiration} + Z \text{ faecal pellets} - \text{remineralization} - \text{sinking} - \text{mixing}$$

The specific functional forms used are:

$$\frac{dN}{dt} = - \frac{N}{e+N} \frac{a}{b+cP} P + \frac{\beta \lambda P}{\mu + P} Z + \gamma dZ + \phi D + k(N_0 - N) \quad (1)$$

$$\frac{dP}{dt} = \frac{N}{e+N} \frac{a}{b+cP} P - rP - \frac{\lambda P}{\mu + P} Z - (s+k)P \quad (2)$$

$$\frac{dZ}{dt} = \frac{\alpha \lambda P}{\mu + P} Z - dZ \quad (3)$$

$$\frac{dD}{dt} = rP + (1 - \alpha - \beta) \frac{\lambda P}{\mu + P} Z - (\psi + \phi + k)D \quad (4)$$

Following SH81, the concentrations N , P , Z and D are given in g C m^{-3} , with concentrations and parameters converted to the appropriate units using the conversion equivalences $1 \text{ g carbon} \equiv 20 \text{ mg chlorophyll} \equiv 10 \text{ mmol nitrogen}$. Time t is measured in days and all parameters are positive. A full description of the NPZ subsection of

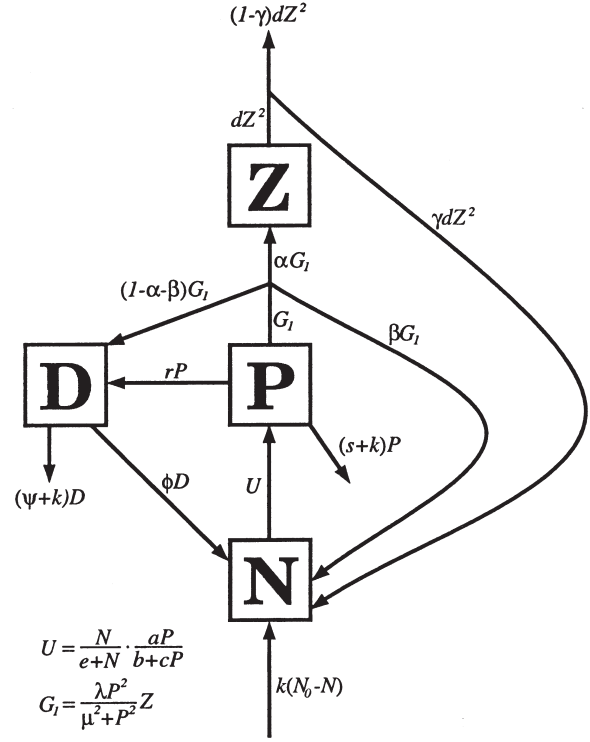


Fig. 1. Interactions between nutrients (N), phytoplankton (P), zooplankton (Z) and detritus (D) for Model 1. Arrows indicate flows of matter through the system, and are labelled with the functions used to model the processes. Open-ended arrows indicate the input to and losses from the system. U is the phytoplankton uptake function and G_1 is the zooplankton grazing term. See Table I for parameter definitions.

the model, based on the models of SH81 and SH93, is given by EB96. Here, we summarize the NPZ subsection of the model and explain the formulation of the additional processes that involve detritus. Each parameter definition is given in Table I, together with a default value (the value originally used by SH81) and a range of values. The ranges cover those used by a variety of authors across a spectrum of models [detailed in EB96, amended slightly by Edwards and Brindley (Edwards and Brindley, 1999)], and will be used later.

Nutrients enter the mixed layer due to diffusive mixing with deep water, which is assumed to have a constant concentration N_0 of nutrients. The mixing occurs at a rate k , which represents the fraction of the mixed layer that is exchanged with deep water each day. Following SH81, we consider a fixed mixed-layer depth of 12.5 m, which is implicitly incorporated into the values of a , k , s and ψ . A shallow mixed layer is characteristic of summertime conditions at stations in the North Atlantic Ocean [e.g. (Fasham, 1993); SH93].

Phytoplankton growth is given by the first term in equation (2), where $N/(e + N)$ represents nutrient limitation

Table I: Parameter definitions, default values and ranges. The ranges are based on values used in a variety of other models

Parameter	Symbol	Default value	Reported range
a/b gives maximum P growth rate	a	0.2 m ⁻¹ day ⁻¹	0.07–0.28
Light attenuation by water	b	0.2 m ⁻¹	0.04–0.2
P self-shading coefficient	c	0.4 m ² (g C) ⁻¹	0.3–1.2
Higher predation on Z	d	1.0 m ³ (g C) ⁻¹ day ⁻¹	0.25–2.0
Half-saturation constant for N uptake	e	0.03 g C m ⁻³	0.02–0.15
Cross-thermocline exchange rate	k	0.05 day ⁻¹	0.0008–0.13
P respiration rate	r	0.15 day ⁻¹	0.05–0.15
P sinking loss rate	s	0.04 day ⁻¹	0.032–0.08
N concentration below mixed layer	N_0	0.6 g C m ⁻³	0.1–2.0
Z growth efficiency	α	0.25	0.2–0.5
Z excretion fraction	β	0.33	0.33–0.8
Regeneration of Z predation excretion	γ	0.5	0.5–0.9
Maximum Z grazing rate	λ	0.6 day ⁻¹	0.6–1.4
Z grazing half-saturation coefficient	μ	0.035 g C m ⁻³	0.02–0.1
D remineralization rate	ϕ	0.1 day ⁻¹	0.004–0.2
D sinking loss rate	ψ	0.08 day ⁻¹	0.08–0.8

with half-saturation constant e , and $a/(b + cP)$ represents non-nutrient-limited growth, which decreases due to light attenuation by the water, b , and by the phytoplankton, c . The value a/b gives the maximum daily growth rate averaged over the depth of the mixed layer. Edwards (Edwards, 1997) has shown how a can be related to the canonical form for primary production derived by Platt *et al.* (Platt *et al.*, 1990) and Platt and Sathyendranath (Platt and Sathyendranath, 1993), giving a formulation of a that allows its value to be calculated explicitly for any location and for any time of the year.

Phytoplankton can be grazed upon by zooplankton, modelled using the Holling Type III function $\lambda P^2/(\mu^2 + P^2)$, with maximum zooplankton grazing rate λ and half-saturation constant μ . A fraction α of zooplankton grazing fuels growth of the zooplankton, and a fraction β is excreted by zooplankton and is regenerated immediately into the nutrient compartment. The remaining fraction $1 - \alpha - \beta$ represents zooplankton faecal pellets, which enter the detritus compartment. In the original NPZ model, faecal pellets were assumed to sink out of the mixed layer and be lost from the system. The rP term is a general phytoplankton loss term, incorporating phytoplankton respiration and natural mortality. For the NPZ model, this was converted straight back into utilizable nutrient, but here this process occurs via remineralization of detritus by bacteria [e.g. (Fasham *et al.*, 1990)]. Phytoplankton can sink out of the mixed layer (and are subsequently lost from the system)

at a rate s , and also get mixed across the base of the mixed layer, at a rate k .

Zooplankton grow by consuming phytoplankton, and are themselves consumed by higher predators. This mortality is modelled using the quadratic function dZ^2 , as proposed by SH81 and SH92, and used by EB96. Zooplankton mortality terms, called ‘closure terms’ by SH92, are implicitly assumed by modellers to include natural mortality. A proportion γ of the mortality term is regenerated as nutrient via excretion of the higher predators, with the remaining fraction $1 - \gamma$ fuelling the growth of the higher predators.

The detritus concentration increases due to the phytoplankton loss rP , and due to faecal pellets from zooplankton grazing on phytoplankton. Detritus can be converted into nutrient via remineralization by (unmodelled) bacteria. This remineralization is modelled as a flow of ϕD converting detritus into nutrient, where the rate ϕ has units of day⁻¹. Detritus can sink out of the mixed layer, given by the term $-\psi D$, where the sinking rate ψ has units of day⁻¹. Detritus will also leave the mixed layer due to mixing with sub-mixed-layer water; as for nutrient and phytoplankton, this linear loss rate is parameterized by k . Following Fasham (Fasham, 1995), we assume that faecal pellets of the higher predators sink out of the mixed layer rapidly, without the possibility of being remineralized within the mixed layer.

We need values for the two parameters ϕ and ψ , which are new to this model and were not present in the NPZ

model. Fasham *et al.* (Fasham *et al.*, 1990) quoted the review of breakdown rates of dead organic matter by Jones and Henderson, who found a range of 0.004–0.18 day⁻¹ (Jones and Henderson, 1986). Fasham *et al.* used the value of 0.05 day⁻¹ for breakdown of detritus into dissolved organic nitrogen, which can then be utilized by phytoplankton via uptake by bacteria. The Hood and Olson closed NPZD model (Davis and Steele, 1994) has a value of 0.2 day⁻¹. To include all these values, we thus take a range for ϕ of 0.004–0.2, with a default at the average value of $\phi = 0.1$ day⁻¹.

Fasham *et al.* used two detritus sinking velocities of 1 and 10 m day⁻¹ (Fasham *et al.*, 1990). Since we have a relatively shallow mixed-layer depth of 12.5 m, we use the lower value for our default sinking velocity. Dividing the sinking velocity by the mixed-layer depth gives a default value for the sinking rate of $\psi = 0.08$ day⁻¹, and a range of 0.08–0.8.

In the Appendix, we summarize the algebraic results that can be obtained for the model. The algebraic approach involves attempting to derive analytical expressions for the steady states (equilibria) of the system, without invoking particular numerical values for the parameters; Truscott and Brindley performed such an

analysis on a general class of NPZ models (Truscott and Brindley, 1994). This insightful exercise enables us to understand some aspects of the dynamics of the model before we undertake any numerical computations; we relate these algebraic results to the numerical calculations within the following sections.

TIME SERIES AND PHASE PORTRAITS

Figure 2a shows the time series of the system from the initial condition $(N, P, Z, D) = (0.4, 0.1, 0.05, 0.08)$, with all of the parameters fixed at their default values. The three-dimensional picture shows the N, P and Z values of the trajectory. The system settles down to steady-state values of $(N, P, Z, D) = (0.33, 0.034, 0.072, 0.060)$; starting from a variety of other initial conditions it does likewise. This steady state is the unique steady state with $N, P, Z, D > 0$, which we know from the analysis given in the Appendix. An equivalent steady state was reached for the NPZ model, with values of $(N, P, Z) = (0.31, 0.034, 0.072)$.

Figure 2b shows that when d , the higher predation on

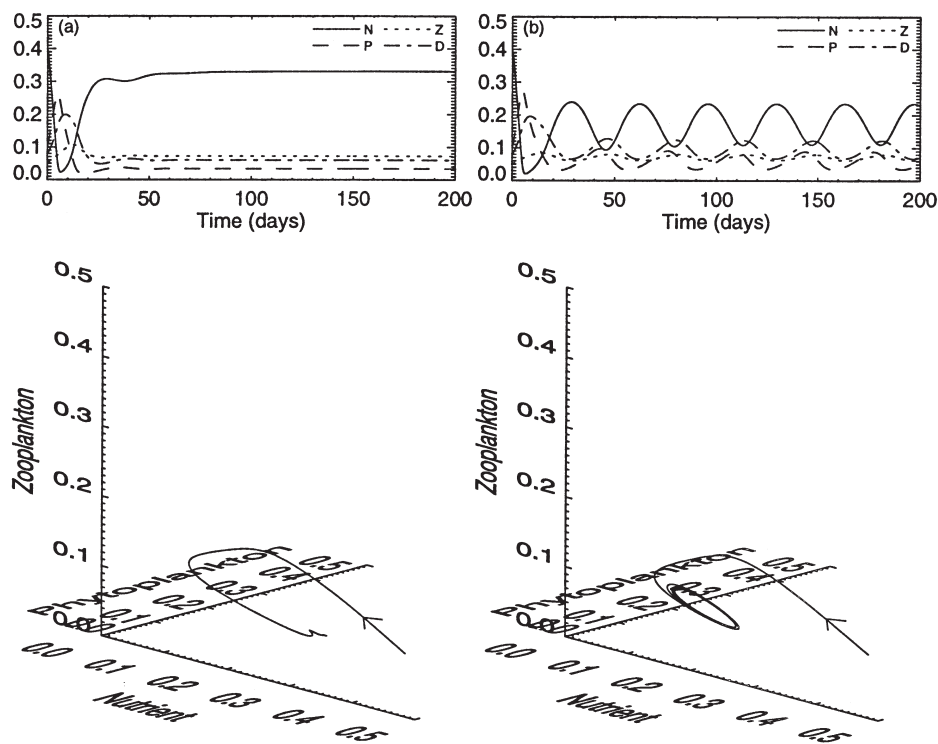


Fig. 2. The time series and trajectory for two values of d , with all of the other parameters fixed at their default values. Each trajectory is shown as the NPZ projection of the full NPZD phase space; all units are g C m^{-3} . (a) For $d = 1.0$ (left diagrams), the trajectory reaches a stable steady state, whereby all four variables remain constant with time. (b) For $d = 1.5$, the trajectory reaches a stable limit cycle, for which all four variables exhibit repeating oscillations.

zooplankton, is increased to 1.5, the variables are not attracted to steady-state values, but rather (after a short transient time) they undergo exactly repeating oscillations: the trajectory is attracted onto a limit cycle. This is what happened for the NPZ model, and the period of the oscillations obtained here is 34 days, only 1 day less than the period for the NPZ model. The existence and nature of such oscillations led to a useful characterization of the dynamics of the NPZ model as parameters were varied (EB96). Therefore, we now follow the same methodology with the $NPZD$ model, to investigate how the addition of the detritus compartment changes the dynamics of the NPZ model. We choose d as the primary parameter to vary because SH81 found it to have a significant effect on the dynamics of their NPZ model (from which our model is derived), and d is a particularly difficult parameter to measure and assign a value to—SH93 stated that in any model it is essentially a free choice.

ONE-PARAMETER BIFURCATION BEHAVIOUR

Figures 2a and b show a clear qualitative difference between the dynamics at the two values of d . Instead of computing a vast gallery of similar time series for various values of d , we now construct bifurcation diagrams. Firstly, consider Figure 3a, showing nutrient values against the parameter d . Figure 2a showed that when $d = 1.0$, the trajectory is attracted to a steady state with $N = 0.33$. This is indicated by the solid line passing through the coordinates ($d = 1.0, N = 0.33$) in Figure 3a; the solid line indicates that the steady state is locally stable, and so attracts, rather than repels, nearby trajectories. At values of $d < 1.0$ and up to the square marked A, the steady state remains stable, but its N value changes.

The limit cycle shown in Figure 2b occurs at $d = 1.5$ in Figure 3a; the maximum and minimum values of N

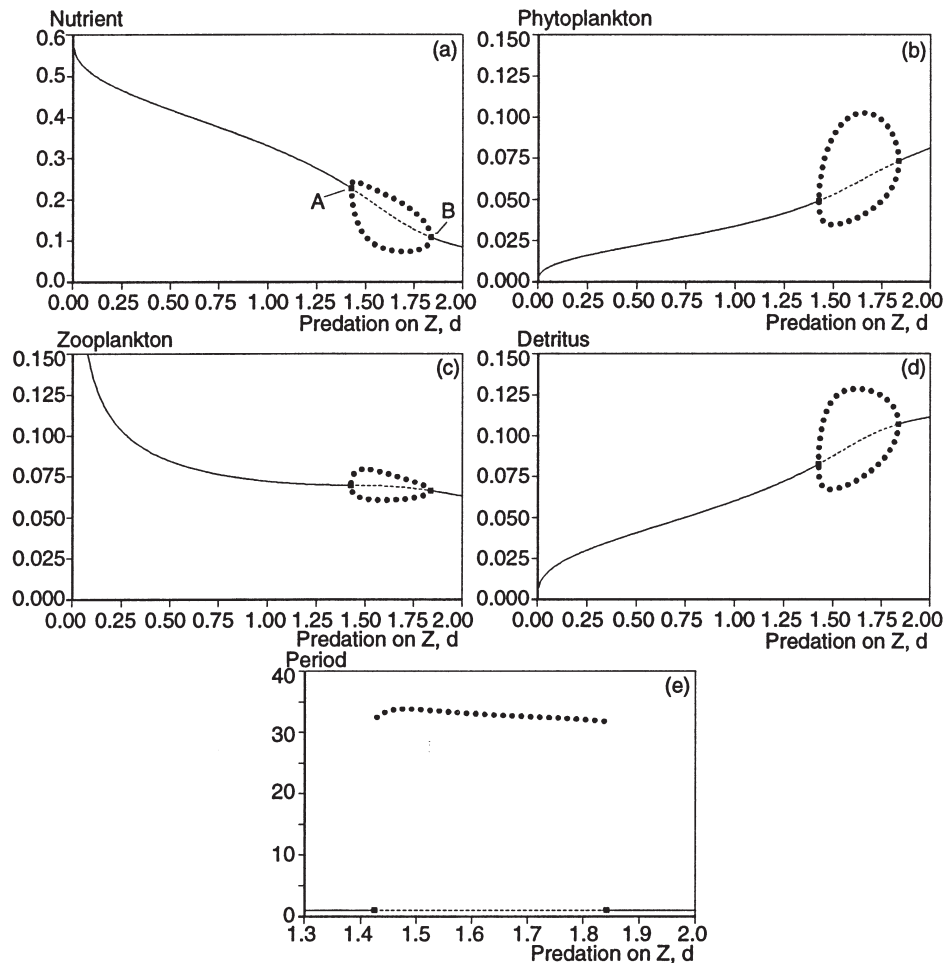


Fig. 3. Variations in the steady-state values of (a) nutrient, (b) phytoplankton, (c) zooplankton and (d) detritus as d , the higher predation on the zooplankton, is changed. A solid line is a stable steady state, a dashed line is an unstable steady state, a solid square is a Hopf bifurcation, and solid circles indicate the maximum and minimum values of the stable limit cycles. In (a), the Hopf bifurcations are labelled A and B. (e) The period (in days) of the limit cycles (solid circles) remains virtually constant throughout the region of oscillatory behaviour; the corresponding stability of the steady state is indicated by the horizontal line. Units of N, P, Z and D are $g\ C\ m^{-3}$, and d is in $m^3(g\ C)^{-1}\ day^{-1}$.

reached during an oscillation are indicated by the solid circles. The dashed line passing through $d = 1.5$ indicates that the steady state still exists, but that it is unstable rather than stable (and so it repels, rather than attracts, nearby trajectories); therefore, it did not attract the trajectory in Figure 2b. The two branches of solid circles show that there exists a stable limit cycle at each value of d between the squares marked A and B, and the N values along the branches show how the maximum and minimum values of N along the limit cycles vary as d changes.

The two squares at the points A and B thus separate the values of d for which trajectories are attracted to steady states or to limit cycles. These points are called Hopf bifurcations [e.g. (Thompson and Stewart, 1986; Glendinning, 1994; Kuznetsov, 1995)]. By definition, they occur at the point where a steady state changes stability and a branch of limit cycles arises. And also by definition, as d varies, the branch of limit cycles collapses (shrinks) onto the steady state at each Hopf bifurcation.

Figures 3b–d show the equivalent bifurcation diagrams for phytoplankton, zooplankton and detritus. Except at low values of d , the steady-state values of Z remain fairly constant as d varies (Figure 3c) and where cycles occur the amplitude of the Z values is small. So, although d is the predation on Z , an increase in d does not greatly decrease the steady-state value of Z (except at low d). But the response of P is much more marked (Figure 3b), with the steady-state values increasing as d increases, and P reaching much higher values along the cycles than for any steady state. The increase in d would not *directly* cause P to increase, rather it would directly cause Z to decrease, releasing some grazing pressure on P which can then increase, causing a reduction in N . The higher P allows Z to consume more, and this higher growth seemingly offsets the expected direct reduction due to the increase in mortality from predators.

Figure 3d shows that the steady-state values of D correlate with those of P . This is to be expected from the definition of the steady-state value of D , given by equation (19) in the Appendix, and by noting that both inputs to the D compartment will increase with P .

The changes in the period of the limit cycles are shown in Figure 3e, with solid circles indicating the period, which is only defined for the appropriate range of d (i.e. between the two Hopf bifurcations). We see that the period remains fairly insensitive to the value of d , and stays close to the value of 34 days seen for the trajectory in Figure 2b.

Equivalent bifurcation diagrams were computed for the NPZ model by EB96, except that there was no detritus diagram. EB96 found that the Hopf bifurcations occurred at $d = 1.42$ and $d = 1.91$, compared with $d = 1.43$ and $d = 1.84$ for the current $NPZD$ model, so oscillations occur across a slightly smaller range of d for the $NPZD$ model. Otherwise, the diagrams are remarkably similar for the

two models, the main dissimilarity being that a larger range of P values is reached for the NPZ model.

Figure 3 was constructed using the dynamical-systems package Auto (Doedel *et al.*, 1994). Auto does not work by computing trajectories at numerous individual values of d to determine whether steady states or limit cycles are reached, but instead utilizes the theory of dynamical systems. It starts from a user-given steady state, then changes d by a small amount, and recomputes the new steady state and its stability. Stability is calculated from the eigenvalues of the Jacobian matrix, also called the community matrix (Murray, 1989). When a Hopf bifurcation is reached (as indicated by the eigenvalues), the branch of limit cycles that emanates from it is then computed.

TWO-PARAMETER BIFURCATION BEHAVIOUR

In Figure 4, we plot two-parameter bifurcation diagrams, which show how the qualitative nature of the diagrams in Figure 3 changes as each of the remaining parameters is varied independently. Each diagram corresponds to a different parameter, with the range shown on the vertical axis being from zero to approximately the maximum reported value given in Table I. The horizontal axis is always d , and a and b have been combined as a/b in a single diagram for the maximum phytoplankton growth rate, giving 14 distinct bifurcation diagrams. The diagrams were computed using the dynamical-systems package LOCBIF (Khibnik *et al.*, 1992, 1993).

For each parameter, the bifurcation diagram from Figure 3 is shown as a horizontal line at the default value of the parameter. The line is horizontal because the parameter was held constant in Figure 3. A solid horizontal line represents a stable equilibrium, a dashed horizontal line is an unstable equilibrium, and squares again represent the Hopf bifurcations, labelled A and B in Figure 4a. In the region of d where the equilibrium is unstable, limit cycles occur, as for Figure 3. In each diagram of Figure 4, the positions of the two Hopf bifurcations are tracked as d and one other parameter are varied. A non-horizontal solid line shows how the d value of the Hopf bifurcation changes as the parameter is varied.

For example, consider Figure 4f, the diagram for the phytoplankton sinking loss rate, s . As s increases from its default value of 0.04 (indicated by the horizontal line) to its maximum value of 0.08, Hopf A moves to the right (its d value increases), and Hopf B moves slightly to the right and then back to the left. As s decreases from 0.04, both Hopf bifurcations move to the left. So both bifurcations persist across the full range of s . The area between the two Hopf bifurcations is where the steady state is unstable and limit cycles occur; outside this region, the steady state is

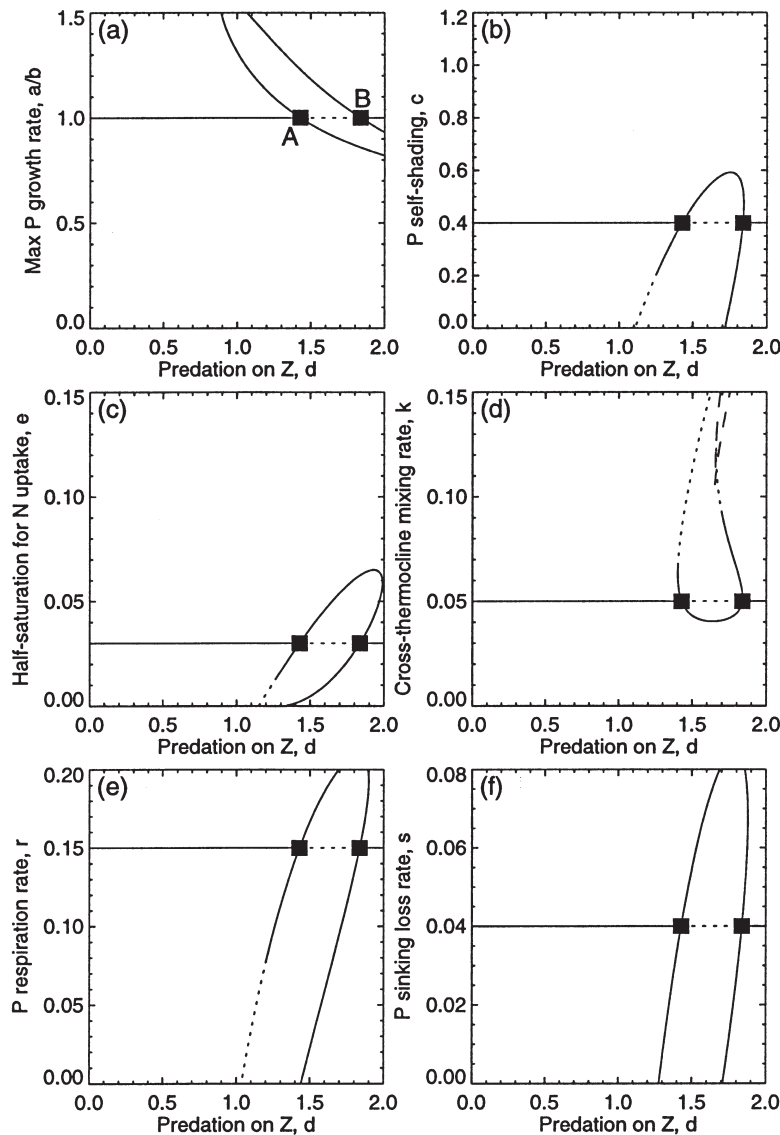


Fig. 4. Two-parameter bifurcation diagrams showing how the positions of the Hopf bifurcations in Figure 3 change as each other parameter, together with d , is independently varied from its default value. The steady-state stabilities from Figure 3 are shown as a horizontal line at each default parameter value. Hopf A and Hopf B are indicated in (a). Non-horizontal solid curves starting from the original Hopf bifurcations (the squares) indicate supercritical Hopf bifurcations, and non-horizontal curves of short dashes show where Hopf bifurcations are subcritical. Essentially, oscillations occur between the lines of Hopf bifurcations, where the steady state is unstable. In (d) and (g), curves of long dashes indicate fold bifurcations of the steady state. Diagrams (a)–(f) are very similar to those shown by EB96 for the original NPZ model. All units are as in Table I.

stable. Thus, limit cycles can occur across the full range of s .

Figure 4j for the regeneration parameter γ shows a similar picture, as does Figure 4e for r . However, in Figure 4e the solid line from Hopf A becomes dashed as r decreases. This indicates where Hopf A becomes subcritical; the solid lines mean that the Hopf bifurcations are supercritical. The technical details of these terms and their consequences are explained in detail by EB96. Essentially, a branch of cycles still commences from a

subcritical Hopf bifurcation, but the cycles are unstable rather than stable, and then these cycles often become stable as d is varied. But here we are more concerned with the overall picture presented by Figure 4, and how it compares with the corresponding picture for the NPZ model.

The three aforementioned diagrams are the only ones for which the Hopf bifurcations persist across the full range of the parameters. Now consider Figure 4b for the self-shading parameter c . Both Hopf bifurcations persist as c decreases, but as c increases they come together at $c = 0.59$,

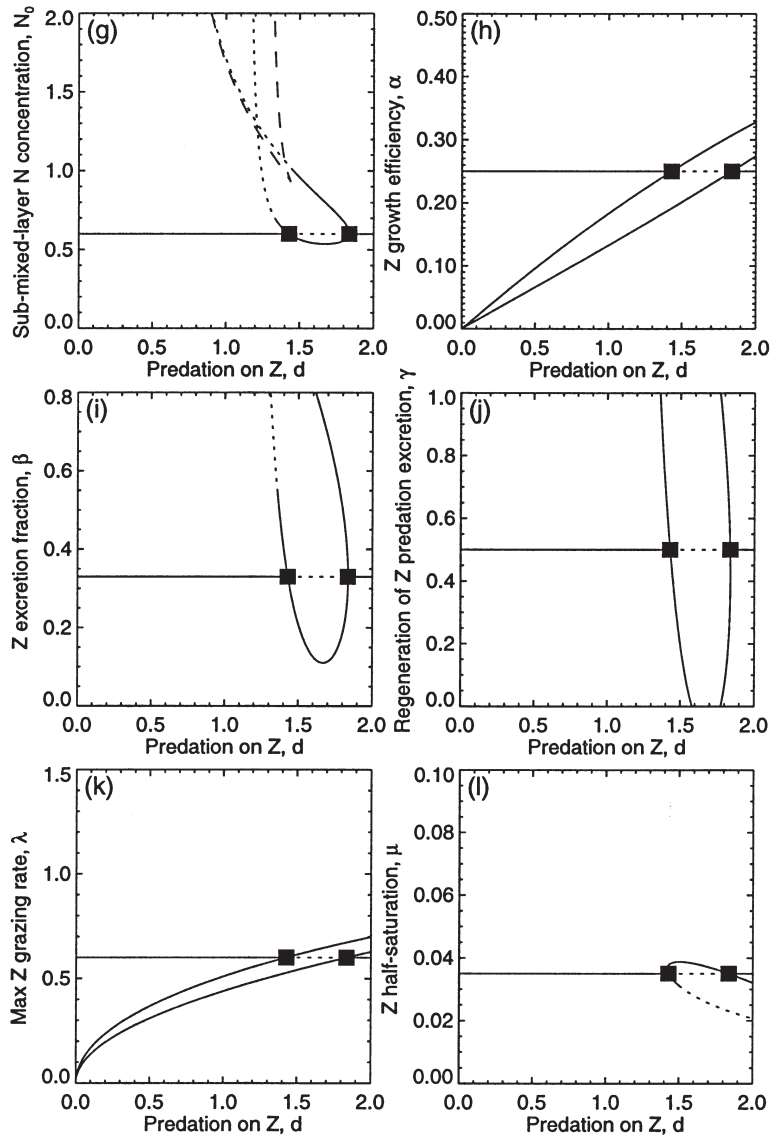


Fig. 4. (g)–(l).

and do not occur above this value. This explains how Figure 3a would change qualitatively with an increase in c . Figure 3a has $c = 0.4$ (the default value). An increase in c would cause Hopf bifurcations A and B to come closer together, giving a shorter and shorter branch of limit cycles, until at $c = 0.59$ both bifurcations would meet and disappear. This would leave just a solid line for the new Figure 3a, indicating that a stable steady state occurs for all values of d , and that no cycles are expected to occur. (Actually, the branch of cycles may itself undergo bifurcations and cycles may still occur above $c = 0.59$, but this does not appear to happen, as discussed in the next section.)

In Figures 4d and g there are curves of long dashes, which indicate fold (also called saddle-node) bifurcations

of the steady state. In the region between the two curves in each diagram, this means that there are three co-existing steady states, two of which may be stable (and hysteresis can occur). For such regions, a trajectory will be attracted to one or other of the two stable steady states, dependent upon the initial conditions assigned to N , P , Z and D , whereas for the default parameters used in Figure 2a, only one stable steady state exists (Figure 3), and this is reached from any initial conditions (with $N, P, Z, D > 0$). Examples of how the equivalent Figure 3a diagram would look when multiple steady states exist were computed by EB96 for the NPZ model.

Figures 4a–l are virtually identical to the equivalent 12 diagrams shown by EB96 for the NPZ model. The

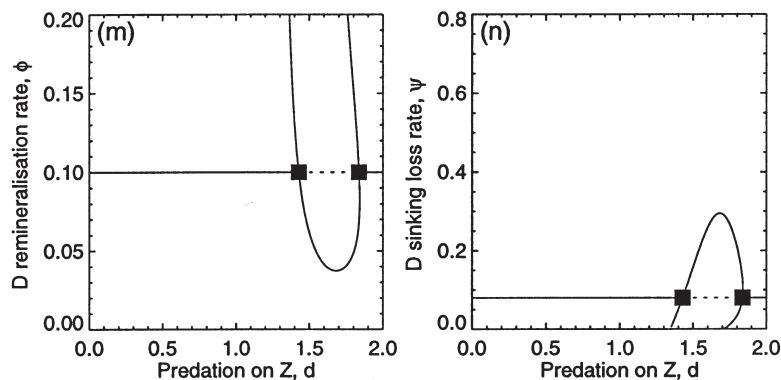


Fig. 4. (m) and (n).

dynamical behaviour of the NPZ model therefore appears to change very little when the D compartment is added to the system. Our computation of bifurcation diagrams shows that the models are similar over broad regions of parameter space—we have not restricted ourselves to looking at variations in only a few parameters. Further details of the diagrams for the NPZ model were discussed by EB96, and since the diagrams for the $NPZD$ model are so similar, we do not give any more details here.

The addition of the detritus equation to the NPZ model introduces an extra eigenvalue of the Jacobian matrix (see Appendix), but despite its potential to alter the stability of steady states, this eigenvalue apparently does not cause any extra bifurcations—it seems to remain negative and not pass through zero. For each diagram of Figure 4 in turn, we have searched for further bifurcations of the steady state. This was done for each parameter by setting $d = 1.0$ and increasing and decreasing the parameter across its full range, and then repeating this at a low and a high value of d . Then the parameter was fixed at a high then a low value, and d varied across its range. No other bifurcations were found, implying that the Hopf and fold bifurcations plotted are indeed the only such bifurcations occurring in the realistic regions of parameter space explored.

We have two more diagrams for Model 1 than for the NPZ model, namely Figures 4m and n for parameters ϕ and ψ (which relate to detritus and so did not appear in the NPZ model). Figure 4m shows that the Hopf bifurcations persist across almost the full range of ϕ , and Figure 4n shows that the bifurcations only occur at low values of ψ . These diagrams tell us how the choice of default values for ϕ and ψ influences our results (a considerable advantage of using our approach to analyse the models). Most values of ϕ

within the range given in Table I would give a qualitatively similar diagram to Figure 3a, whereas oscillations do not occur at high values of ψ .

DEPENDENCE OF THE PERIOD OF OSCILLATIONS ON THE PARAMETER VALUES

Figure 2b showed that the limit cycle obtained when $d = 1.5$ has a period of 34 days. Figure 3e then showed that the period remains close to this value as d is varied between the values of the two Hopf bifurcations. In Figure 5, we show how the period changes as ϕ and ψ are varied. Figures 4m and n are redrawn (for a smaller range of d), and within the regions of oscillations contours of constant period (measured in days) are plotted. Contours are plotted at increments of 5 days, and are computed using a method described elsewhere (Edwards and Brindley, 1999). The squares indicate Hopf bifurcations A and B at the default values of ϕ and ψ . The diagrams show that the period can range from just below 30 days to values no greater than 40 days, as ϕ or ψ are varied (the 40-day contour lies above the realistic range of ϕ). Thus, the values of ϕ and ψ do not greatly affect the period of the oscillations.

Edwards and Brindley plotted such contour diagrams for all 12 parameters in the NPZ model, and found that the period does not reach as low as 20 days, and can exceptionally attain values >100 days (Edwards and Brindley, 1999). We have investigated whether or not the effect on the period of varying each of the remaining 12 parameters in the $NPZD$ model is the same as for the NPZ model. This was done by criss-crossing the region of oscillations for each parameter (Edwards, 1997). We

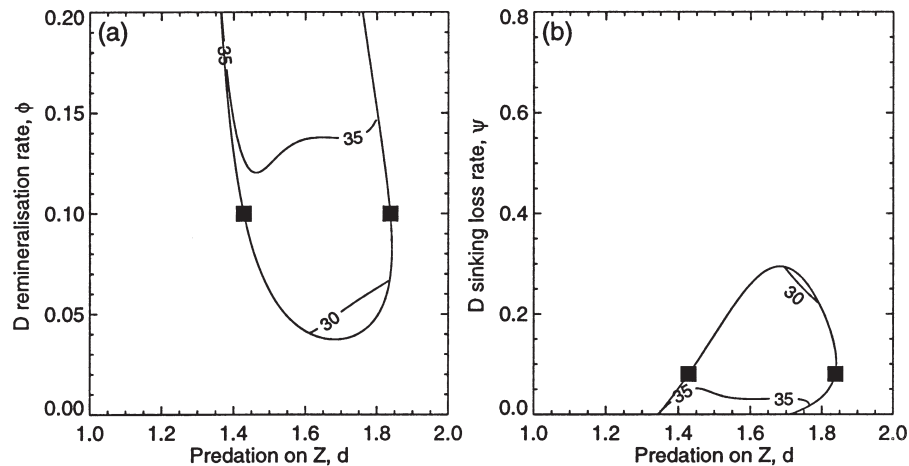


Fig. 5. Within the regions of oscillations given by Figures 4m and n, for the parameters ϕ and ψ which do not occur in the NPZ model, the variations in period of the stable limit cycles are given by contours of constant period. The contours are plotted at increments of 5 days. Black squares indicate the Hopf bifurcations at the default parameter values. For each of the remaining parameters, the period varies in a similar way as for the NPZ model.

found that the period changes fairly conclusively in the same manner as for the NPZ model, i.e. if an increase in a parameter increases the period for the NPZ model, then this is also true for the $NPZD$ model. Even when the actual region of oscillations is fairly narrow, as in Figures 4h and k for α and λ , the trend of the period still agrees with that for the NPZ model. In general, the period remains within a narrower range for the $NPZD$ model than for the NPZ model. One clear difference is that for variations in β , the period remains below 50 days for the $NPZD$ model, but can reach >125 days for the NPZ model (albeit for a very narrow range of d). This difference is due to homoclinic connections occurring for the NPZ model (Edwards, 1997), which arise from a Bogdanov–Takens bifurcation, but this is beyond the scope of the present paper [although see Scheffer *et al.* for a clear graphic example of how such dynamics appear commonplace for their simple PZ model, and indeed can explain abrupt changes in ecosystem state (Scheffer *et al.*, 2000)].

The clear conclusion from the results concerning Model 1 (including the Appendix) is that the simple addition of detritus to the NPZ model does not significantly affect the nature of the bifurcations. The analytical and numerical investigations demonstrate that the general bifurcational structure of the NPZ model is preserved upon addition of the detritus compartment in the manner presented here. This implies that if an ecosystem is considered to be expressed by the food web shown in Figure 1, and knowledge of the actual level of detritus is not explicitly required, then the dynamics of the food web may be modelled by considering just the NPZ system.

With hindsight, it may be unsurprising that the addition of the detritus compartment to the NPZ model does not greatly affect the dynamics, because D only appears linearly in the equations for the model. However, it would not seem possible to have predicted, a priori, that this should be the case. Rather, once the investigation has been performed, the fact that D only appears linearly in the equations offers a plausible explanation for the unaltered dynamics.

MODEL 2—ZOOPLANKTON GRAZING ON DETRITUS PLUS PHYTOPLANKTON

We now modify Model 1 to give Model 2, in which zooplankton can graze on both detritus and phytoplankton. As mentioned in the Introduction, this is a feature of some models in the literature, but not of others. This modification adds extra interactions to the food web, and requires changing the zooplankton grazing function of Model 1 to incorporate consumption of the two alternative food sources, phytoplankton and detritus.

M. J. R. Fasham (personal communication) suggested the following function for zooplankton grazing on phytoplankton, as used by Ryabchenko *et al.* (Ryabchenko *et al.*, 1997):

$$G = \frac{\lambda \beta P^{\lambda} Z}{\beta \mu + \beta P^{\lambda} + \beta D} \quad (5)$$

where parameters β_1 and β_2 are assumed nominal preferences [termed ‘palatabilities’ by Evans (Evans, 1988)] for

phytoplankton and detritus when the concentrations of these foods are equal. Thus, an increase in the preference for detritus, p_2 , or in detritus itself, will directly reduce the grazing pressure on phytoplankton as the zooplankton switch to the more preferable or relatively more abundant food source. The equivalent function for zooplankton grazing on detritus is:

$$G_2 = \frac{\lambda p_2 D^2 \zeta}{\mu + p_1 P + p_2 D} \quad (6)$$

By dividing through equations (5) and (6) by p_1 and defining

$$\omega = \frac{p_2}{p_1}$$

as the relative zooplankton palatability for detritus compared to phytoplankton, we obtain the final grazing functions:

$$G_1 = \frac{\lambda P^2 \zeta}{\mu + P + \omega D}$$

$$G_2 = \frac{\lambda \omega D^2 \zeta}{\mu + P + \omega D}$$

Setting $\omega = 0$ means that $p_2 = 0$, such that zooplankton do not find detritus palatable at all, corresponding to Model 1 for which G_1 reduces to the original $\lambda P^2 \zeta / (\mu^2 + P^2)$ form, and $G_2 = 0$.

The resulting new food web is shown in Figure 6. Allowing zooplankton to graze on detritus creates the extra pathway from D to Z , plus the resulting recyclings of excretion into N , given by βG_2 , and of faecal pellets back into D , $(1 - \alpha - \beta)G_2$. The remainder of the food web is the same as for Model 1, except for the dependence of G_1 on D . Following Fasham *et al.* (Fasham *et al.*, 1990), we use the same values of α and β for zooplankton grazing on detritus as for grazing on phytoplankton.

The resulting equations for the model are:

$$\begin{aligned} \frac{dN}{dt} &= - \text{uptake} + \zeta \text{ excretion} + \zeta \text{ predation excretion} + \\ &\quad D \text{ remineralization} + \text{mixing} \\ \frac{dP}{dt} &= \text{uptake} - \text{respiration} - \text{grazing by } \zeta - \text{sinking} - \\ &\quad \text{mixing} \\ \frac{d\zeta}{dt} &= \text{growth} - \text{higher predation} \\ \frac{dD}{dt} &= P \text{ respiration} + \zeta \text{ faecal pellets} - \text{grazing by } \zeta - \\ &\quad \text{remineralization} - \text{sinking} - \text{mixing} \end{aligned}$$

The specific functional forms used are:

$$\frac{dN}{dt} = - \frac{N}{c+N} - \frac{a}{b+cP} P + \frac{\beta \lambda (P^2 + \omega D^2) \zeta}{\mu + P + \omega D} + \gamma d \zeta + \phi D + k(N_0 - N) \quad (7)$$

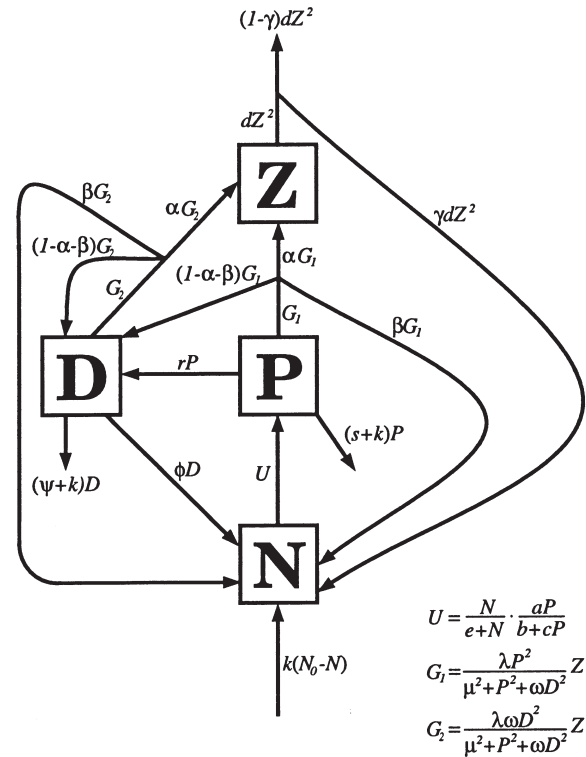


Fig. 6. For Model 2, zooplankton graze on detritus as well as on phytoplankton, adding extra pathways to the system. G_2 is the function for zooplankton grazing on detritus. As with grazing on phytoplankton, a proportion α fuels zooplankton growth, β is excreted and $(1 - \alpha - \beta)$ is returned to detritus as faecal pellets. The grazing-on-phytoplankton function, G_1 , now depends on D as well as P and ζ .

$$\frac{dP}{dt} = \frac{N}{c+N} - \frac{a}{b+cP} P - \quad (8)$$

$$rP - \frac{\lambda P^2 \zeta}{\mu + P + \omega D} - (s+k)P$$

$$\frac{d\zeta}{dt} = \frac{\alpha \lambda (P^2 + \omega D^2) \zeta}{\mu + P + \omega D} - d\zeta \quad (9)$$

$$\frac{dD}{dt} = rP + \frac{[(1 - \alpha - \beta)P^2 - (\alpha + \beta)\omega D] \lambda \zeta}{\mu + P + \omega D} - (\phi + \psi + k)D \quad (10)$$

The $(1 - \alpha - \beta)P^2$ term in the numerator of the second term of equation (10) represents zooplankton faecal pellets that are the result of feeding on phytoplankton, as for Model 1. The $-(\alpha + \beta)\omega D^2$ term represents the net loss of detritus due to zooplankton feeding on detritus: detritus is lost due to zooplankton grazing by an amount G_2 , where $G_2 = \lambda \omega D^2 \zeta / (\mu^2 + P^2 + \omega D^2)$, but an amount $(1 - \alpha - \beta)G_2$ is then returned to detritus as faecal pellets, giving the net result $-G_2 + (1 - \alpha - \beta)G_2 = -(\alpha + \beta)G_2$.

The incorporation of multiple zooplankton grazing into the model only adds one extra parameter, ω , to the

system. Fasham had zooplankton grazing on phytoplankton, detritus and bacteria, for which the respective nominal preference values used were $p_1 = 0.5$, $p_2 = 0.25$ and $p_3 = 0.25$, where p_3 is the nominal preference for bacteria (Fasham, 1993). Popova *et al.* did not model bacteria, and took $p_1 = 0.7$ and $p_2 = 0.3$ (Popova *et al.*, 1997). We use Fasham's values for $\omega = p_2/p_1$, to give a default value of $\omega = 0.5$. The zooplankton palatability for phytoplankton is therefore assumed to be twice that for detritus. We take a range of $\omega \in [0, 2]$, so that the maximum value gives the converse situation to the default, in that the palatability for detritus is twice that for phytoplankton.

In the Appendix, we present the analytical results concerning steady states of Model 2. The extra terms introduced into the equations, compared with those for Model 1, mean that explicitly calculating a positive steady state of the form (N^*, P^*, ζ^*, D^*) is even more difficult for Model 2 than for Model 1.

TIME SERIES AND PHASE PORTRAITS

Figure 7a shows the time series and trajectory (as an NPZ projection) of the system from the initial condition $(N, P, \zeta, D) = (0.4, 0.1, 0.05, 0.08)$, with all of the parameters

fixed at their default values. The system settles down to a steady state with values $(N^*, P^*, \zeta^*, D^*) = (0.36, 0.035, 0.091, 0.036)$. Comparing these values to the equivalent steady state for Model 1, given by $(N^*, P^*, \zeta^*, D^*) = (0.33, 0.034, 0.072, 0.060)$, we see that the steady state for Model 2 has slightly higher values of N^* and P^* , and increase in ζ^* of 26%, and a reduction in D^* of 41%. The changes in ζ^* and D^* are the expected direct result of allowing the zooplankton to graze on the detritus. The minor increase in P^* from that of Model 1 may be expected, since the zooplankton now have an alternative source of food to phytoplankton. However, when the system is at the steady state, the loss rate of phytoplankton due to zooplankton grazing, given by the different definitions of G_1 in each model, is higher for Model 2 than for Model 1. So, the zooplankton are grazing more phytoplankton per day than in Model 1, but P^* is actually higher. This can be explained by the small increase in N^* , which is due to increased regeneration from excretion. It is interesting to note that nutrient limitation to phytoplankton growth is given by $N/(e + N)$, and although the N^* values of 0.33 and 0.36 are well above the half-saturation constant value of $e = 0.03$, the difference in N^* values between the models does seem to influence the value of P^* .

The transient time taken to reach the steady state is

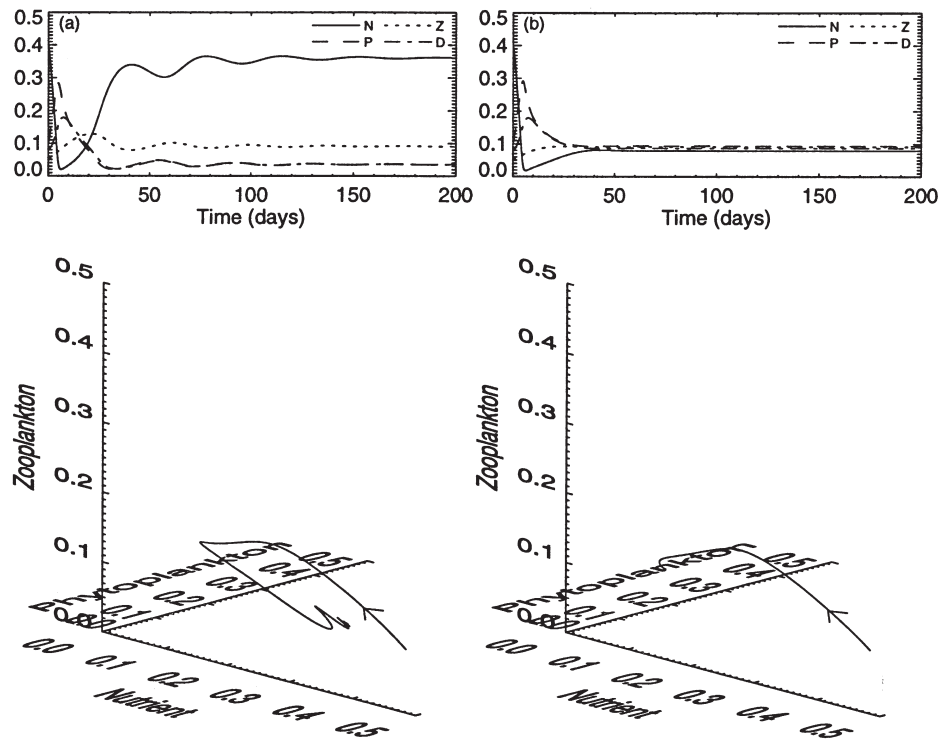


Fig. 7. The time series and trajectory for Model 2 at (a) $d = 1.0$ and (b) $d = 1.5$, with all of the other parameters fixed at their default values. For $d = 1.5$, the system settles down to a steady state, in contrast to Model 1 and the NPZ model.

longer than for Model 1. This is because the eigenvalues (of the Jacobian matrix) with real parts closest to zero, which for both models are a complex and conjugate pair, have the real part equal to -0.078 for Model 1, whereas for Model 2 the real part is -0.022 . This means that the steady state in Model 2 is less strongly attracting, and hence the transient time is longer. Starting from a host of other initial conditions, all trajectories converge onto the same steady state, implying that $(N, P, Z, D) = (0.36, 0.035, 0.091, 0.036)$ is the unique steady state with strictly positive values of all four variables. Unlike Model 1, we could not verify this by mathematical analysis (see the Appendix).

In Figure 7b, we show what happens when d is set to 1.5. A steady state is reached, for which all four variables take

roughly equal values. This behaviour is unlike Model 1 and the original NPZ model, for which a stable limit cycle occurs when $d = 1.5$. Whether or not the limit cycles of Model 1 have disappeared, because of the extra interactions introduced for Model 2, will now be investigated by computation of one-parameter bifurcation diagrams.

ONE-PARAMETER BIFURCATION BEHAVIOUR

Figure 8 shows how the steady-state values of the variables vary with d . More significantly, they show that limit cycles do occur, and have not been eliminated by the slight change in model structure from Model 1. The oscillations

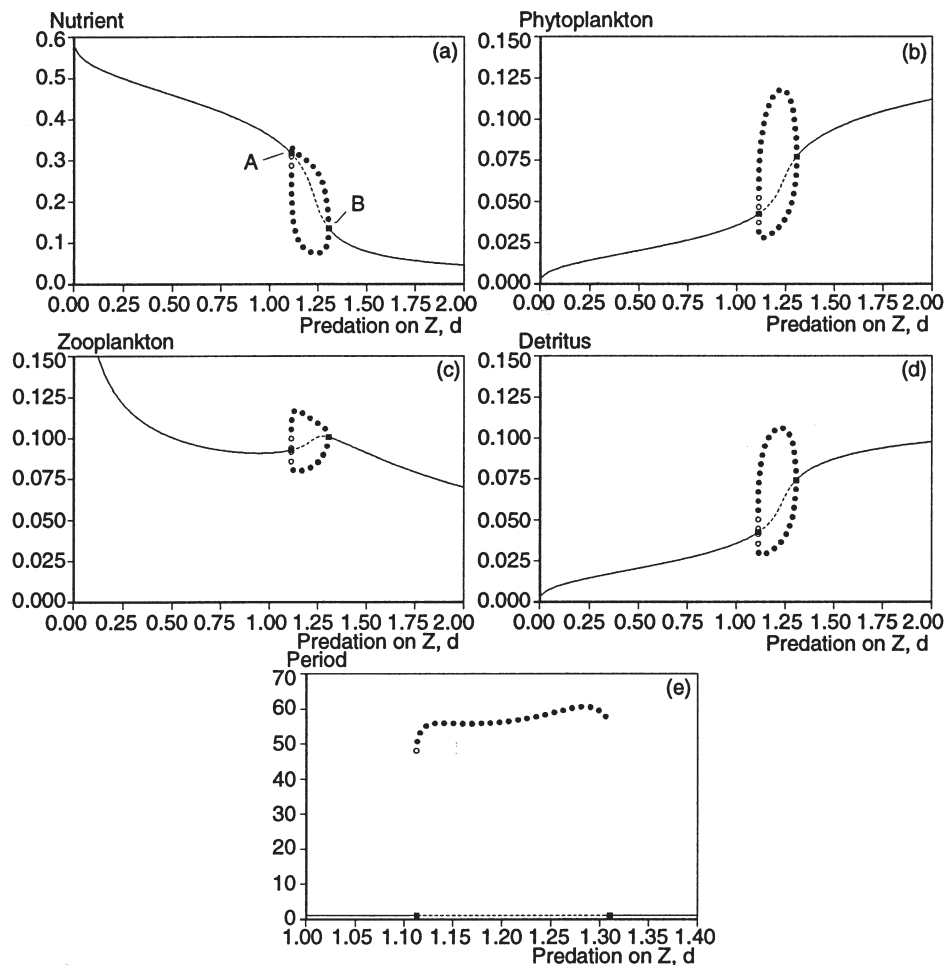


Fig. 8. Variations in the Model 2 steady-state values of (a) nutrient, (b) phytoplankton, (c) zooplankton and (d) detritus as d is varied. The key is the same as for Figure 3, and open circles represent unstable cycles, which only occur close to the subcritical Hopf A and are not of great importance (see the text). The stable oscillations do occur, but over a narrower range of d than for Model 1. (e) The period of the stable limit cycles varies between 48 and 61 days. These are higher periods than shown in the equivalent Figure 3e for Model 1, and the range of the periods is greater, despite the interval of d values that exhibits oscillations being smaller.

occur at lower d values, and across a much narrower range of d values, than for Model 1. The Hopf bifurcations A and B occur at $d = 1.11$ and $d = 1.31$, compared with $d = 1.43$ and $d = 1.84$ for Model 1. Hopf bifurcation A is sub-critical, rather than supercritical, meaning that the branch of limit cycles emanating from it is unstable rather than stable—the corresponding maxima and minima of the cycles are represented by the open circles. This branch then undergoes a fold bifurcation, resulting in a branch of stable limit cycles (solid circles), which eventually collapse onto Hopf B as d increases. The fact that Hopf A is sub-critical is not too important, and simply leads to a very narrow region of d values (between the fold bifurcation of the cycles and Hopf A) for which a stable limit cycle, an unstable cycle and a stable steady state all co-exist. A trajectory will reach one of the two stable attractors depending on the initial conditions. Unstable cycles will not be reached (because they are unstable and so repel nearby trajectories), and are mentioned for mathematical completeness rather than ecological importance.

Comparing Figures 8a and 3a, we see that at values of d above Model 2's Hopf B, N^* is lower for Model 2 than for Model 1, whereas at values of d below Model 2's Hopf A, N^* is higher for Model 2. The lowest minimum values of N reached along a cycle are similar for both models, but higher maximum values are attained for Model 2.

From Figures 8b and 3b, we see that at values of d below Hopf A, P^* is fairly similar for both models, but for values above Hopf B in Model 2, P^* is much higher than for Model 1. It even reaches higher values than the maximum values of P along the limit cycles in Model 1. In both Model 1 and the NPZ model, the maximum P values along the cycles exceed the highest P^* value reached, whereas such high values are reached by the steady state in Model 2.

As expected, we see from Figures 8c and 3c that the values of Z^* are greater for Model 2 (an expected result because the zooplankton have more food sources). Also, the values of Z during the oscillations are higher than those attained both during the cycles and at steady states for Model 1.

From Figures 8d and 3d, we see that D^* is usually lower for Model 2 than for Model 1. This would be expected, due to the consumption of detritus by zooplankton in Model 2. However, for $d \in (1.32, 1.43)$, the steady state is stable for both models, and D^* is actually greater in Model 2. This curious effect demonstrates that the non-linearities and feedback loops in these models mean that the expected outcome of an alteration does not always occur, i.e. letting zooplankton eat the detritus will not always reduce the detritus concentration. Similar 'unexpected effects' were investigated by Yodzis in the context of perturbation experiments on ecological communities that lie

in equilibrium (Yodzis, 1981, 1988). The region of d for which D^* is greater in Model 2 than in Model 1 lies to the right of the oscillatory region for Model 2, but to the left of the oscillatory region for Model 1. So that fact that the oscillations have shifted along, as indicated by the d values of the Hopf bifurcations moving, may be seen as a warning that the quantitative nature of the steady states may change significantly.

Finally, Figure 8e shows that the period of the oscillations ranges between 48 and 61 days as d varies. This is greater variation than in Figure 3e for Model 1 (note the change in scales), despite the range of d values being smaller. The period remains at higher values than those shown in the equivalent Figure 3e for Model 1, indicating that allowing the zooplankton to graze on the detritus causes a slowing down of the oscillations.

In Figure 9, we illustrate the trajectory for $d = 1.25$, the value halfway between the two values of Figure 7. A limit cycle is reached, which is to be expected from Figure 8. The cycle has a period of 59 days, much longer than the period of 34 days attained by the limit cycle at $d = 1.5$ for Model 1. We already know this, as well as the amplitudes of the oscillations, from Figure 8.

So the oscillations have not disappeared, rather the

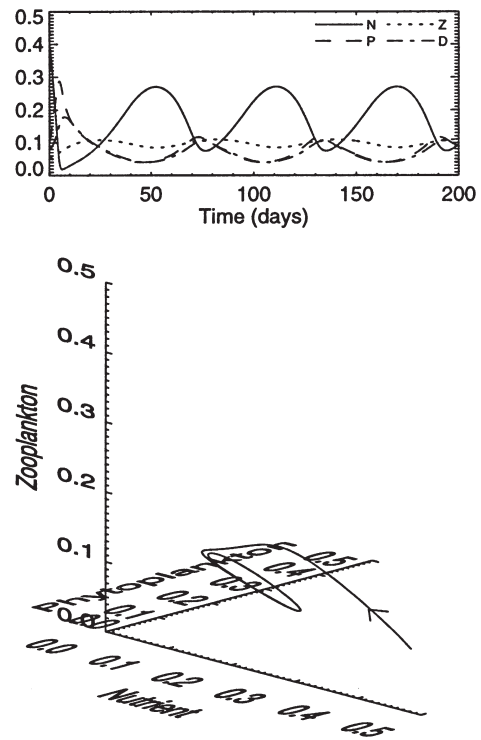


Fig. 9. Time series and trajectory showing the nature of the oscillations for $d = 1.25$. The period is 59 days, which we already know from Figure 8e; this is longer than any period for Model 1 when all parameters except d are set to their default values, as shown by Figure 3e.

range of d values for which they occur has been shifted and shrunk, compared to Model 1, and the period has lengthened.

TWO-PARAMETER BIFURCATION BEHAVIOUR

Since two Hopf bifurcations occur for Model 2, we can construct equivalent two-parameter bifurcation diagrams to those for Model 1 given in Figure 4. These diagrams are shown in Figure 10. The most striking difference between the diagrams for Model 1 and Model 2 is that the regions of oscillations are much narrower for Model 2. This is not surprising, since Figure 8 showed that the oscillations occur over a much narrower range of d (with all other parameters fixed at their default values) than for Model 1. However, despite this narrower range of d , the pictures for each parameter are still qualitatively similar for the two models: the oscillations tend to persist or not persist, as each parameter is varied, in the same way for both models.

The most informative diagram is Figure 10o for ω , the zooplankton feeding preference, a parameter which does not appear in Model 1. Recall that $\omega = 0$ means that zooplankton do not graze on detritus at all, and so $\omega = 0$ corresponds to Model 1. Thus, in Figure 10o, the d values of the Hopf bifurcations at $\omega = 0$ are the default d values of the Hopf bifurcations in Model 1. We see that a very small increase in ω from zero causes Hopf B to move to the left (its d value decreases) by a significant amount. Hopf A initially moves to the right as ω increases from zero, and then it moves to the left. At $\omega = 0.05$, Hopf A is again at $d = 1.43$, the same value as for $\omega = 0$, but at $\omega = 0.05$, Hopf B has moved to $d = 1.62$, compared to the value of $d = 1.84$ at $\omega = 0$. The value of $\omega = 0.05$ means that the zooplankton preference for phytoplankton is 20 times their preference for detritus, but even this small predilection for detritus has an impact on the dynamics, compared to the $\omega = 0$ situation of complete distaste for detritus.

Hopf A is supercritical at $\omega = 0$, and remains so as ω increases, until $\omega = 0.39$ where it becomes subcritical. This explains why in Figure 8, for which $\omega = 0.5$, Hopf A is subcritical. As ω increases further, the Hopf bifurcations remain practically the same distance apart, and move only slightly to the left. Thus, at such values, the qualitative behaviour is fairly insensitive to the value of ω , whereas at the low values small changes in ω can have large consequences. Fold bifurcations of the steady state occur at high values of ω (there are actually two curves of fold bifurcations, which terminate at a cusp point at $\omega = 1.56$, although the curves are very close together and look like just one curve in Figure 10o).

The diagrams for each of the parameters are similar to those for Model 1, despite the narrower regions of oscillations and the fact that Hopf A is subcritical at the default values in Model 2. For example, Figures 10b and 4b show that, for both models, oscillations do not occur for c greater than ~ 0.6 , and can occur at all values < 0.6 . Oscillations occur across the full ranges of r , s and γ for both models. The fact that at the default parameters the oscillations occur across only a small range of d in Model 2 makes it surprising that the oscillations should still persist across the full ranges of these parameters, and that the bifurcation diagrams in general remain so similar between the two models.

In Figure 10j, fold bifurcations of the steady state occur at high values of γ , but these did not occur for Model 1. This can be explained because fold bifurcations occur at high levels of ω , and so if we had instead computed the bifurcation diagrams with ω set to a high default value, fold bifurcations would appear in each of the diagrams. So, at the default value of $\omega = 0.5$, the fold bifurcations start ‘creeping in’ to some of the diagrams.

The diagrams that show the most striking difference between the two models are Figure 10l and Figure 4l for μ , the half-saturation constant for zooplankton grazing. This is not too surprising, since G_1 (the function for zooplankton grazing on phytoplankton) has changed definition from Model 1, effectively replacing μ^2 with $\mu^2 + \omega D^2$, and the introduction of G_2 (the function for zooplankton grazing on detritus) means that μ appears elsewhere in the equations. In Figure 10l, we see that the two curves of Hopf bifurcations cross over, and fold bifurcations of the steady state occur. The two fold curves terminate at a cusp point. This looks quite different to the equivalent picture (Figure 4l) for Model 1, but in actual fact the picture for Model 1 is qualitatively the same as that for Model 2, but is shifted to the right, outside of the plotted range of d (the cusp point of the curves of fold bifurcations occurs at $d = 2.26$). So Figure 10l and Figure 4l are not as qualitatively different as first appears.

The other parameters involved in the zooplankton grazing functions are α , β and λ . The corresponding bifurcation diagrams for these parameters show the same qualitative nature between the two models (except that the fold bifurcations for β in Model 1 occur out of the range plotted). Figure 10m shows that oscillations can now occur across the whole range of ϕ , the remineralization rate of detritus, whereas the oscillations do not occur at low values of ϕ for Model 1.

So, overall, the general qualitative nature of the bifurcational structure of Model 1, and of the NPZ model, is retained upon the introduction of multiple grazing by zooplankton, but there are significant quantitative changes.

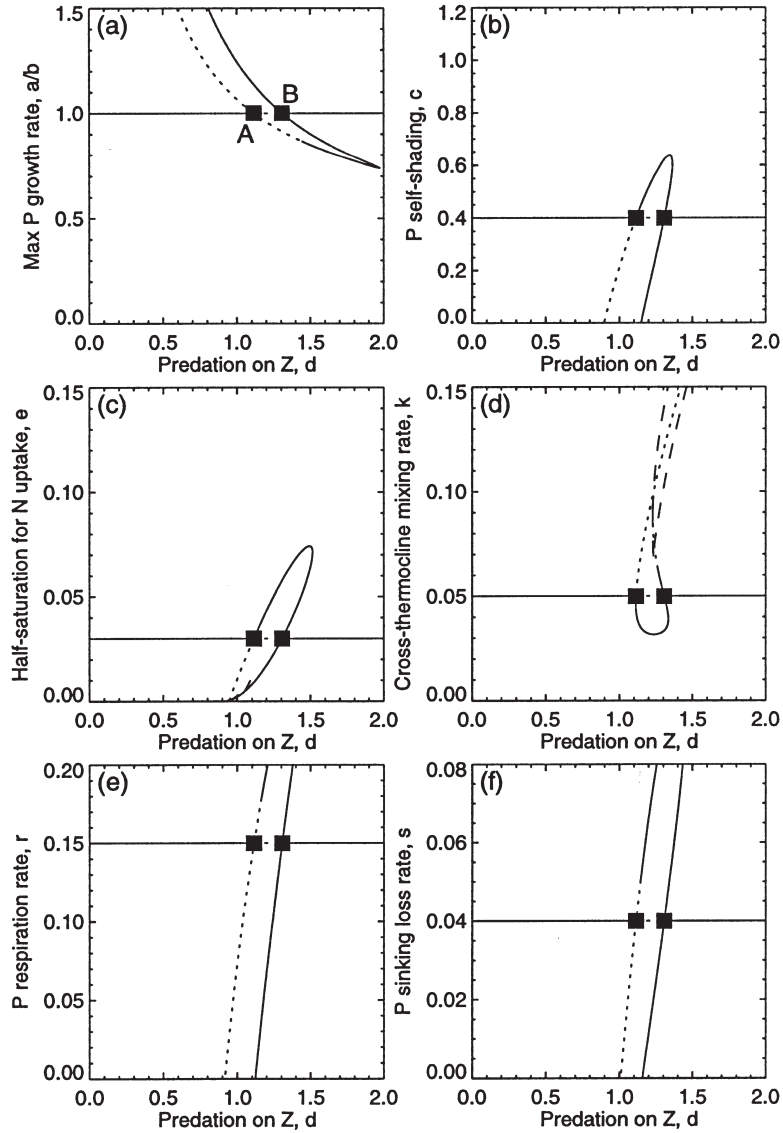


Fig. 10. Two-parameter bifurcation diagrams showing how the positions of the Hopf bifurcations in Figure 8 change as each other parameter, together with d , is independently varied from its default value. The key is the same as for Figure 4. In the extra diagram (o) for ω , $\omega = 0$ corresponds to Model 1. At small values of ω , the Hopf bifurcations are shifted to the left and get closer together, shrinking the region of oscillations, but then the d values do not change greatly as ω increases.

DEPENDENCE OF THE PERIOD OF OSCILLATIONS ON THE PARAMETER VALUES

In Figure 11, we show the period–contour diagrams for ϕ , ψ and ω , the three parameters that appear in Model 2 but not in the NPZ model. Figure 8e showed that as d changes, and the other parameters are set to their default values, the period of the oscillations varies between 48 and 61 days. Thus, we know a priori that there must be 50-

55- and 60-day contours passing through the default values of each of the parameters in the three diagrams of Figure 11.

We first discuss Figure 11c for the zooplankton feeding preference, ω ; note that we have plotted d from 0.8 to 1.8, rather than from 1.0 to 2.0, in order to show the full behaviour. Since $\omega = 0$ corresponds to Model 1, there is, as expected, a 35-day contour close to $\omega = 0$. Figure 11c shows that as ω increases from zero, the period of the oscillations increases quite sharply at first, attaining >50 days when ω has only reached $\omega = 0.2$. As ω increases

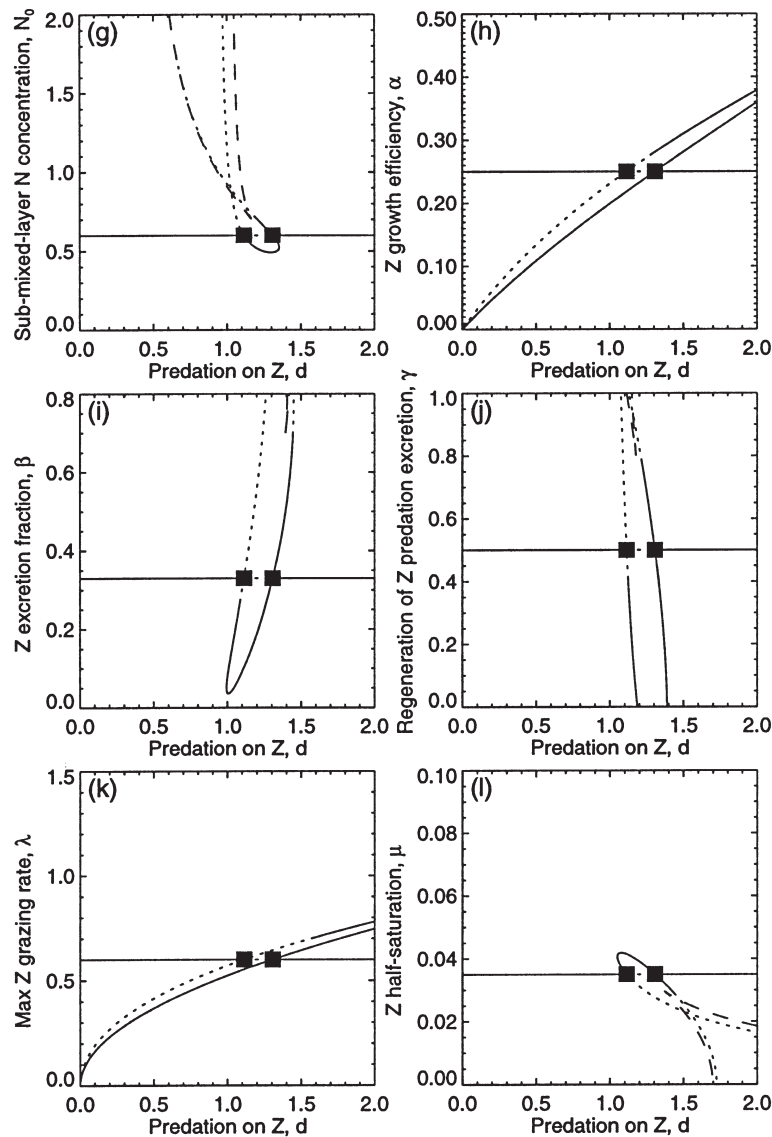


Fig. 10. (g)-(l).

further, the period is between 55 and 65 days for most values of d , but at values of d close to Hopf B, higher periods are reached, as indicated by the closely compacted contours. The highest contour reached is for a period of 100 days.

The left-hand endpoints of the 50 and 55 contours are fold bifurcations of the limit cycles (mentioned earlier). This must be so since at the corresponding values of ω Hopf A is subcritical (and therefore the branch of cycles emanating from it is unstable, but the contours only represent the period of stable cycles). The closeness of the two endpoints to the curve of subcritical Hopf bifurcations

shows that the region of co-existence of a stable limit cycle with a stable fixed point, defined as the region lying between the Hopf bifurcations and the fold bifurcations of the limit cycles, is very small. Thus, the region of oscillations is bounded, more or less, by the curves of Hopf bifurcations. This is important in interpreting the two-parameter bifurcation diagrams of Figure 10, and means that we can talk of the oscillatory region as being, as near as makes no great difference, the region bounded by the curves of Hopf bifurcations. So, the fact that Hopf A is subcritical rather than supercritical in Figure 8 and in regions of Figure 10 is not too important.

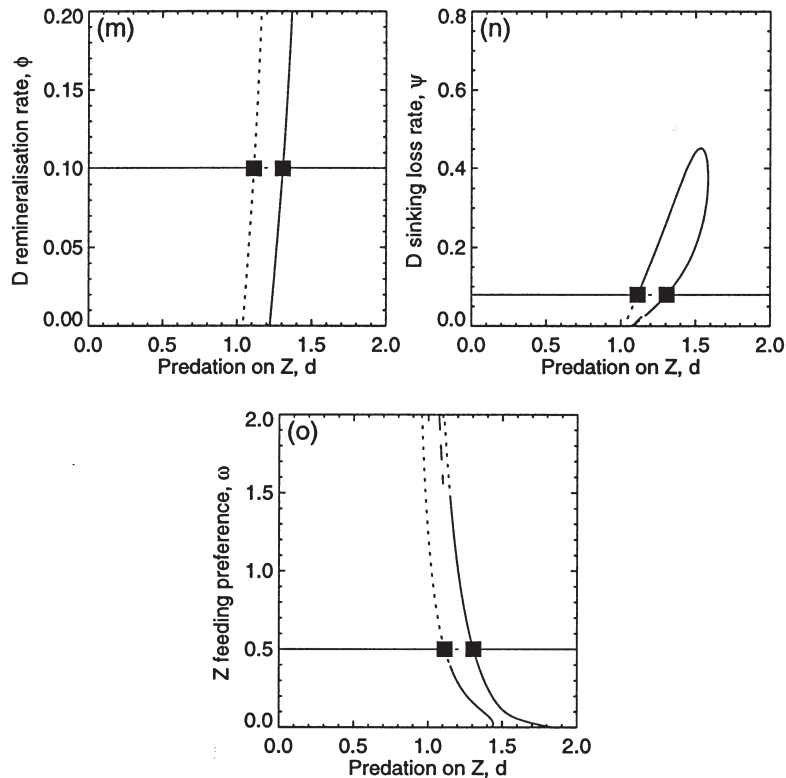


Fig. 10. (m)–(o).

Figure 11a shows that as the detritus remineralization rate, ϕ , increases, the period tends to increase. This was also the case for Model 1. Since, as already mentioned, there must be 50-, 55- and 60-day contours passing through the default value of ϕ , the fact that no other contours appear in the diagram (the 45 and 65 contours lie outside of the plotted range) implies that the variation of period with ϕ is as small as possible. Furthermore, the 50 and 55 contours are practically vertical and remain very close to Hopf A, and so away from Hopf A the period remains around 60 days.

Figure 11b for the detritus sinking loss rate, ψ , shows much more variation in the period than Figure 11a for ϕ . For Model 1, the variation for ψ was the same as that for ϕ , although the actual range of ψ exhibiting oscillations is smaller for Model 1 than for Model 2. At high values of ψ , the period becomes as low as 35 days, and at values approaching zero it reaches 150 days.

Using the same approach as for Model 1, we have verified whether or not the period changes in the same direction as for the NPZ model when each of the other parameters is increased and decreased. The starting point we used for each parameter was the limit cycle that occurs for $d = 1.21$, which is the midpoint of the region of

oscillations, with all of the other parameters set to their default values. This cycle has a period of 57 days.

As for Model 1, we find that the period tends to vary with each parameter in the same direction as that for the NPZ model. The situation for β is not as clear-cut as for the other parameters, with the 60-day contour running almost the full length (in a vertical direction) of the oscillatory region, whereas for the NPZ model the contours tend to be horizontal. At the maximum value of $\beta = 0.75$, the period reaches 89 days, much higher than that attained at low levels of β . So, in agreement with the behaviour of the NPZ model, the greatest periods are reached at the high values of β . For e , there is also a 60-day contour running from low to high values of e , and there is no clear trend in the period as e varies. For the remaining parameters, the period does behave in the same qualitative way as for the NPZ model and Model 1.

During the process of tracing limit cycles when constructing the contour diagrams here and for Model 1, no bifurcations of limit cycles were found, except for the aforementioned fold bifurcations, which must occur when a Hopf bifurcation is subcritical. So, as for the NPZ model, no period-doubling bifurcations or Naimark–Sacker bifurcations (Kuznetsov, 1995) were

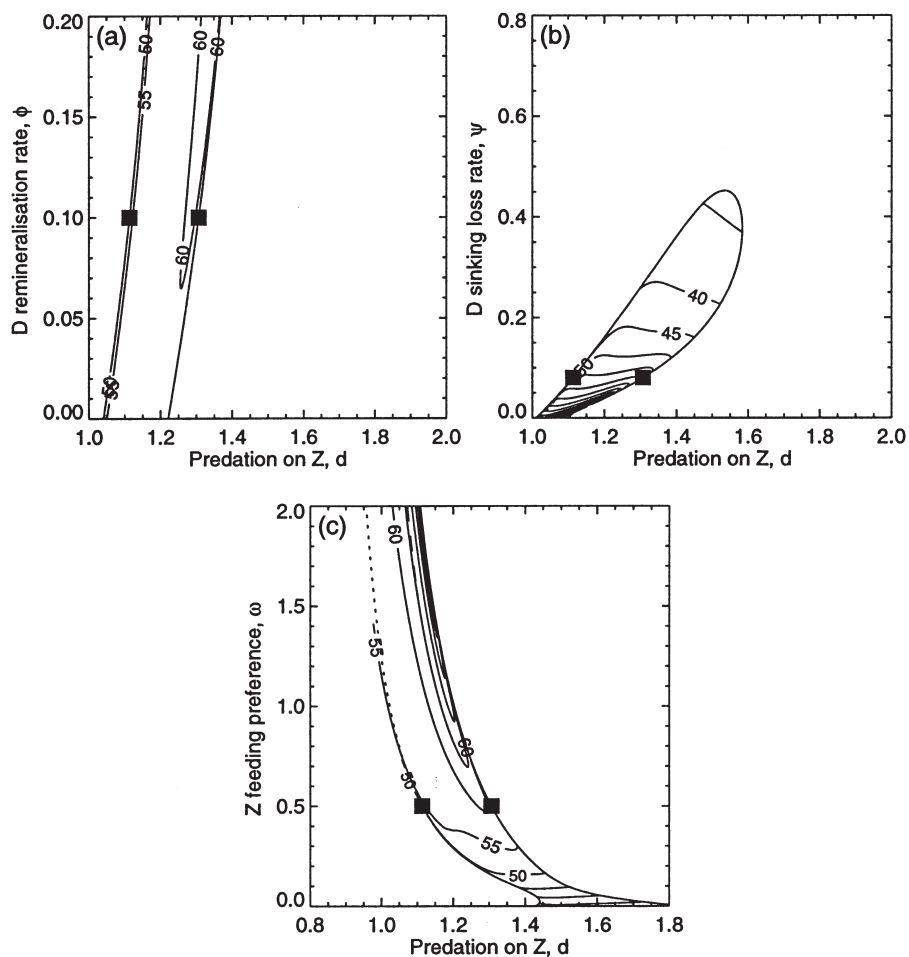


Fig. 11. The period–contour diagrams for each of the parameters ϕ , ψ and ω , which do not appear in the NPZ model, show higher periods than the diagrams for ϕ and ψ for Model 1. As ω decreases to zero, the period reduces to 35 days, corresponding to Model 1.

found anywhere within the oscillatory regions. This means that we have not found the start of a sequence of period-doubling bifurcations which would culminate in a chaotic attractor, and no chaotic behaviour has been found for either $NPZD$ model.

DISCUSSION

We have examined the behaviour of two $NPZD$ models in order to help understand the factors that most influence the dynamics of such models. This work extends earlier work (Edwards and Brindley, 1996), which showed how unforced oscillations in an NPZ model persist as parameters are varied. Here we have added a detritus compartment to simulate remineralization more realistically. First, we examined Model 1, which did not allow zooplankton to graze upon detritus. The resulting diagrams show that the addition of the detritus compartment

hardly changes the nature of the qualitative dynamics that were found for the NPZ model (at least across the regions of parameter space examined). This implies that if the food web of Model 1 represents an ecosystem to be modelled, but the size of the detritus pool is not a required output, then the NPZ model can be used—little is gained by adding the detritus compartment to the NPZ model.

However, the results concerning Model 2 show that if zooplankton are assumed to graze on the detritus, then the dynamics are shifted quantitatively compared to the NPZ model. In this situation, simulations of the full $NPZD$ model are needed, even if knowledge of the value of detritus is not explicitly required—just using the NPZ model as a simplification would not be suitable. Even if zooplankton have only a slight predilection for detritus, the dynamics are shifted, as shown by Figure 10o. The qualitative dynamics found for the NPZ model and Model 1 are preserved for Model 2, but the oscillations occur

across narrower ranges of parameter space and have longer periods.

Edwards and Brindley (Edwards and Brindley, 1999) replaced the zooplankton mortality term dZ^2 in the original NPZ model with the linear form qZ , which is the other popular choice of closure term (Steele and Henderson, 1992). They found that oscillations still occur, and that the oscillations appear to exist across broader ranges of parameter values than for the original NPZ model, and hence than for the models examined here. This implies that changing the zooplankton mortality term from quadratic to linear has more of an effect on the dynamical behaviour of the system than adding the detritus compartment to the NPZ model. It may have been expected that adding a whole new compartment would have more of an effect than just changing one function in the equations. Our results are in keeping with Steele and Henderson, who concluded that the choice of zooplankton mortality term has a large influence upon the output of models (Steele and Henderson, 1992). Edwards and Yool (Edwards and Yool, 2000) recently revealed an anomaly in the models of Steele and Henderson (Steele and Henderson, 1992), but nevertheless their work agreed with and strengthened Steele and Henderson's conclusions. Note, however, that our Figures 4 and 10 show that some of the parameters involved in the 'internal' processes, such as zooplankton grazing, also have a strong influence on the dynamics. This last point highlights a benefit of the approach taken here, namely that sensitivity to every parameter in a model is considered.

Popova *et al.* also investigated the behaviour of an NPZD model (Popova *et al.*, 1997). Their model included seasonal physical forcing of the ecosystem, and was a reduced version of the seven-component Fasham model (Fasham, 1993). Popova *et al.* looked at complex behaviour of the variables, defined as long-term quasi-periodic or chaotic motion, i.e. simulations that did not give an annually repeating cycle of the variables (which would have corresponded to the frequency of the annually repeating forcing) or a repeating cycle with a period of a fixed whole number of years.

Popova *et al.* found the occurrence of complex behaviour to be uninfluenced by the values of parameters related to the half-saturation constant for nitrogen uptake by phytoplankton, phytoplankton mortality rate, detritus remineralization rate and detritus sinking velocity (their Figure 7). Complex behaviour occurred across the full range of each of these parameters, which relate to ϵ , r , ϕ and ψ in our models. Popova *et al.* included zooplankton grazing on detritus, and so our Model 2 corresponds more closely to their model than does our Model 1. In our Figure 10 for Model 2, we see that r and ϕ have little influence upon the existence of oscillations, analogous to

Popova *et al.*'s insensitivity of complex behaviour to these parameters. Insensitivity to these parameters across models is rather desirable, since at present they are almost impossible to measure accurately (Fasham and Evans, 1995). But we note that if seasonal forcing is included in our models, then r plays an important role in determining the annual dynamics (Edwards, 1997), due to its appearance in the function Φ , which is defined here in the Appendix. The other parameters that we found to be fairly uninfluential on the existence of oscillations, namely s , β and γ , were either not included or not varied by Popova *et al.*

On the other hand, we found that the values of the aforementioned parameters ϵ and ψ had more effect upon our oscillations (Figure 10) than Popova *et al.*'s equivalent parameters did on their complex behaviour. So these parameters do not appear to have a definitive influence across models. Differences in model formulation, parameter values and investigational approaches do make such comparisons difficult, and although similarities in results can be revealing, variations are inevitable.

Popova *et al.* found short-term oscillations to be a common feature of their model during the summertime, when the environment is relatively constant and the forcing is weak. Furthermore, for a chaotic trajectory (which thus did not exactly repeat itself year after year), they plotted the probability, for each day of the year, that the first phytoplankton bloom of the year occurred on that day. As would be expected, the most common timing of the bloom was around the abrupt shallowing of the mixed layer in the spring. However, if the bloom did not occur at this time, then it would only occur at certain fixed times, namely 1, 2, 3, 4 or 5 months after the shallowing (and sometimes not until the autumn deepening). So no blooms ever occurred 1.5 months after the shallowing, but they did occur exactly 1 and 2 months after. This intriguing feature points to some monthly periodicity inherent in the dynamics; how this relates to the oscillations of the same period found here and elsewhere (Edwards and Brindley, 1996, 1999; Yool, 1998) remains to be answered.

We have not found any chaotic behaviour here for our unforced models. Caswell and Neubert (Caswell and Neubert, 1998) showed that the chaotic 'tea-cup' attractor of the Hastings and Powell (Hastings and Powell, 1991) three-species food chain still occurs when a quadratic zooplankton mortality term replaces the linear term originally used by Hastings and Powell. Edwards and Bees (Edwards and Bees, 2001) have presented a chaotic attractor for the EB96 NPZ model (which uses the quadratic mortality term), so in general the quadratic mortality term used in this paper does not necessarily eliminate chaos. Owing to the similarities of behaviour between our NPZD

models and the original NPZ model, we suspect that chaos lurks somewhere for our $NPZD$ models, but we have not come across it here.

McCann and Hastings (McCann and Hastings, 1997) also modified the Hastings and Powell (Hastings and Powell, 1991) model, by including omnivory by the top predator. They found that increasing the strength of omnivory tended to stabilize the food web, in the sense that chaotic dynamics and limit cycles tended to be eliminated or be bounded further away from zero population levels. In going from Model 1 to Model 2, we have also found that omnivory reduces the prevalence of limit cycles. These results run counter to the conventional view that omnivory tends to destabilize food webs (Pimm and Lawton, 1978). However, our Figure 10o shows that although a small amount of omnivory does lessen the existence of limit cycles, further increases in the omnivory have little qualitative effect. Similarly, McCann *et al.* found weak interactions to have an important influence on the dynamics of simple food web models (McCann *et al.*, 1998). Recently, Armstrong analysed the stability of models containing multiple phytoplankton species grazed upon by a grazing community that was represented by a single variable (Armstrong, 1999). Stability was enhanced when the grazing preferences for different phytoplankton species could change more rapidly; this is somewhat analogous to our findings just discussed.

Yool (Yool, 1998) examined numerous progressively reduced versions of the Fasham (Fasham, 1993) model, and found detritus to play a key role in the success of the reduced versions in reproducing faithful simulations of the full Fasham model. In particular, an $NPZD$ model was found to reproduce the features of the full Fasham model, but the NPZ model that omitted the detritus compartment exhibited qualitatively different dynamics. Yool allowed zooplankton to graze on detritus in addition to phytoplankton (because Fasham did in the full model), and so his results are consistent with ours, in that adding detritus to our NPZ model to give our Model 2 does affect the dynamics. Yool's simulations, however, show a far more drastic change in dynamics than we find for our models.

It is impractical to attempt to classify the dynamics of plankton models throughout the entire expanse of realistic parameter space. The approach taken here gives us a digestible indication of the nature of the dynamics, and a conception of how the dynamics change with parameter values, functional forms and the number of modelled compartments. Although we have inferred that if oscillations persist in the same way for two models then these models can be said to have similar behaviour, it may be the case that quantitatively the dynamics are actually different (e.g. steady-state values may change significantly). However, the

one-parameter diagrams presented here (Figures 3 and 8) and by Edwards and Brindley (Edwards and Brindley, 1996) do indeed suggest that similarity in the location of Hopf bifurcations is a good indication that steady-state values remain relatively unchanged, whereas if the Hopf bifurcations do move as parameters vary, then the steady-state values do change. The models investigated here do not include any physical forcing, but when such forcing is added to the models, our analytical and numerical results explain features of the annual cycle, such as the presence or absence of a spring phytoplankton bloom (Edwards, 1997). Complex behaviour, as discussed earlier with reference to Popova *et al.* (Popova *et al.*, 1997), was not found when forcing was included in our $NPZD$ models.

Unforced oscillations have proved to be a robust feature of our models. As well as being interesting in their own right (Ryabchenko *et al.*, 1997), their persistence has allowed us to use techniques from the theory of dynamical systems to construct diagrams such as those in Figures 4 and 10. These diagrams can be thought of as giving a broad representation of each model's dynamics across parameter space, and provide a way of determining the effects of changing the formulation of the models. Together with other techniques, such as non-linear optimization (Fasham and Evans, 1995) and data assimilation (Franks, 1997; Fennel *et al.*, 2001), this approach improves our perception of which factors are the most important in controlling the dynamics of plankton population models.

ACKNOWLEDGEMENTS

I am grateful to John Brindley, my thesis supervisor, plus Trevor Platt, Andrew Yool and the referees for their advice and comments. I thank John Steele and Mike Fasham for helpful discussions concerning formulation of the models; these discussions took place at the 1996 Mathematical Modelling of Plankton Population Dynamics symposium, held at the Isaac Newton Institute in Cambridge. This work was funded by the William Wright Smith Scholarship from the University of Leeds, and an NSERC Visiting Fellowship in a Canadian Government Laboratory, held at the Bedford Institute of Oceanography. The Cambridge Philosophical Society partly sponsored my stay at the Isaac Newton Institute.

REFERENCES

- Armstrong, R. A. (1999) Stable model structures for representing biogeochemical diversity and size spectra in plankton communities. *J. Plankton Res.*, **21**, 445–464.
- Busenberg, S., Kumar, S. K., Austin, P. and Wake, G. (1990) The dynamics of a model of a plankton–nutrient interaction. *Bull. Math. Biol.*, **52**, 677–696.

- Caswell, H. and Neubert, M. G. (1998) Chaos and closure terms in plankton food chain models. *J. Plankton Res.*, **20**, 1837–1845.
- Davis, C. S. and Steele, J. H. (1994) Biological/physical modelling of upper ocean processes. Woods Hole Oceanographic Institution Technical Report, WHOI-94-32.
- Denman, K. L. and Peña, M. A. (1999) A coupled 1-D biological/physical model of the northeast subarctic Pacific Ocean with iron limitation. *Deep-Sea Res. II*, **46**, 2877–2908.
- Doedel, E., Wang, X. and Fairgrieve, T. (1994) AUTO: Software for continuation and bifurcation problems in ordinary differential equations. Applied Mathematics Report, California Institute of Technology.
- Edwards, A. M. (1997) A rational dynamical-systems approach to plankton population modelling. PhD Thesis, University of Leeds, Leeds, UK.
- Edwards, A. M. and Bees, M. A. (2001) Generic dynamics of a simple plankton population model with a non-integer exponent of closure. *Chaos, Solitons & Fractals*, **12**, 289–300.
- Edwards, A. M. and Brindley, J. (1996) Oscillatory behaviour in a three-component plankton population model. *Dyn. Stabil. Syst.*, **11**, 347–370.
- Edwards, A. M. and Brindley, J. (1999) Zooplankton mortality and the dynamical behaviour of plankton population models. *Bull. Math. Biol.*, **61**, 303–339.
- Edwards, A. M. and Yool, A. (2000) The role of higher predation in plankton population models. *J. Plankton Res.*, **22**, 1085–1112.
- Edwards, C. A., Batchelder, H. P. and Powell, T. M. (2000a) Modeling microzooplankton and macrozooplankton dynamics within a coastal upwelling system. *J. Plankton Res.*, **22**, 1619–1648.
- Edwards, C. A., Powell, T. A. and Batchelder, H. P. (2000b) The stability of an NPZ model subject to realistic levels of vertical mixing. *J. Mar. Res.*, **58**, 37–60.
- Evans, G. T. (1988) A framework for discussing seasonal succession and coexistence of phytoplankton species. *Limnol. Oceanogr.*, **33**, 1027–1036.
- Evans, G. T. and Parslow, J. S. (1985) A model of annual plankton cycles. *Biol. Oceanogr.*, **3**, 327–347.
- Fasham, M. J. R. (1993) Modelling the marine biota. In Heimann, M. (ed.), *The Global Carbon Cycle*. Springer-Verlag, Berlin, pp. 457–504.
- Fasham, M. J. R. (1995) Variations in the seasonal cycle of biological production in subarctic oceans: A model sensitivity analysis. *Deep-Sea Res. I*, **42**, 1111–1149.
- Fasham, M. J. R., Ducklow, H. W. and McKelvie, S. M. (1990) A nitrogen-based model of plankton dynamics in the oceanic mixed layer. *J. Mar. Res.*, **48**, 591–639.
- Fasham, M. J. R. and Evans, G. T. (1995) The use of optimization techniques to model marine ecosystem dynamics at the JGOFS station. *Philos. Trans. R. Soc. London Ser. B*, **348**, 203–209.
- Fennel, K., Losch, M., Schröter, J. and Wenzel, M. (2001) Testing a marine ecosystem model: Sensitivity analysis and parameter optimization. *J. Mar. Syst.*, **28**, 45–63.
- Flierl, G. R. and Davis, C. S. (1993) Biological effects of Gulf Stream meandering. *J. Mar. Res.*, **51**, 529–560.
- Franks, P. J. S. (1997) Models of harmful algal blooms. *Limnol. Oceanogr.*, **42**, 1273–1282.
- Franks, P. J. S. and Walstad, L. J. (1997) Phytoplankton patches at fronts: A model of formation and response to wind events. *J. Mar. Res.*, **55**, 1–29.
- Franks, P. J. S., Wroblewski, J. S. and Flierl, G. R. (1986) Behavior of a simple plankton model with food-level acclimation by herbivores. *Mar. Biol.*, **91**, 121–129.
- Glendinning, P. (1994) *Stability, Instability and Chaos: An Introduction to the Theory of Nonlinear Differential Equations*. Cambridge Texts in Applied Mathematics. Cambridge University Press, Cambridge.
- Hastings, A. and Powell, T. (1991) Chaos in a three-species food chain. *Ecology*, **72**, 896–903.
- Hilborn, R. and Mangel, M. (1997) *The Ecological Detective: Confronting Models with Data*. Monographs in Population Biology. Vol. 28. Princeton University Press, Princeton, NJ.
- Hofmann, E. E. and Ambler, J. W. (1988) Plankton dynamics on the outer southeastern U.S. continental shelf. Part II: A time-dependent biological model. *J. Mar. Res.*, **46**, 883–917.
- Jones, R. and Henderson, E. W. (1986) The dynamics of nutrient regeneration and simulation studies of the nutrient cycle. *J. Conseil*, **43**, 216–236.
- Khibnik, A. I., Kuznetsov, Y. A., Levitin, V. V. and Nikolaev, E. V. (1992) *Interactive LOCAL BIFurcation Analyzer*. Computer Algebra Netherlands, The Netherlands.
- Khibnik, A. I., Kuznetsov, Y. A., Levitin, V. V. and Nikolaev, E. V. (1993) Continuation techniques and interactive software for bifurcation analysis of ODEs and iterated maps. *Physica D*, **62**, 360–371.
- Kuznetsov, Y. A. (1995) *Elements of Applied Bifurcation Theory*. Applied Mathematical Sciences. Vol. 112. Springer-Verlag, New York.
- McCann, K. and Hastings, A. (1997) Re-evaluating the omnivory–stability relationship in food webs. *Proc. R. Soc. London Ser. B*, **264**, 1249–1254.
- McCann, K., Hastings, A. and Huxel, G. R. (1998) Weak trophic interactions and the balance of nature. *Nature*, **395**, 794–798.
- McCauley, E. and Murdoch, W. W. (1987) Cyclic and stable populations: plankton as paradigm. *Am. Nat.*, **129**, 97–121.
- Murray, J. D. (1989) *Mathematical Biology*. Biomathematics. Vol. 19. Springer-Verlag, Berlin.
- Olson, D. B. and Hood, R. R. (1994) Modelling pelagic biogeography. *Prog. Oceanogr.*, **34**, 161–205.
- Oschlies, A. and Garçon, V. (1998) Eddy-induced enhancement of primary production in a model of the North Atlantic Ocean. *Nature*, **394**, 266–269.
- Oschlies, A. and Garçon, V. (1999) An eddy-permitting coupled physical–biological model of the North Atlantic. 1. Sensitivity to advection numerics and mixed layer physics. *Global Biogeochem. Cycles*, **13**, 135–160.
- Paffenhöfer, G. A. and Knowles, S. C. (1979) Ecological implications of fecal pellet size, production and consumption by copepods. *J. Mar. Res.*, **37**, 35–49.
- Paffenhöfer, G. A. and Strickland, J. D. H. (1970) A note on the feeding of *Calanus helgolandicus* on detritus. *Mar. Biol.*, **5**, 97–99.
- Pimm, S. L. and Lawton, J. H. (1978) On feeding on more than one trophic level. *Nature*, **275**, 542–544.
- Platt, T. and Sathyendranath, S. (1993) Estimators of primary production for interpretation of remotely sensed data on ocean color. *J. Geophys. Res.*, **98**, 14561–14576.
- Platt, T., Sathyendranath, S. and Ravindran, P. (1990) Primary production by phytoplankton: analytic solutions for daily rates per unit area of water surface. *Proc. R. Soc. London Ser. B*, **241**, 101–111.
- Popova, E. E., Fasham, M. J. R., Osipov, A. V. and Ryabchenko, V. A.

(1997) Chaotic behaviour of an ocean ecosystem model under seasonal external forcing. *J. Plankton Res.*, **19**, 1495–1515.

Ryabchenko, V. A., Fasham, M. J. R., Kagan, B. A. and Popova, E. E. (1997) What causes short-term oscillations in ecosystem models of the ocean mixed layer? *J. Mar. Syst.*, **13**, 33–50.

Scheffer, M., Rinaldi, S. and Kuznetsov, Y. A. (2000) Effects of fish on plankton dynamics: a theoretical analysis. *Can. J. Fish. Aquat. Sci.*, **57**, 1208–1219.

Steele, J. H. and Henderson, E. W. (1981) A simple plankton model. *Am. Nat.*, **117**, 676–691.

Steele, J. H. and Henderson, E. W. (1992) The role of predation in plankton models. *J. Plankton Res.*, **14**, 157–172.

Steele, J. H. and Henderson, E. W. (1993) The significance of interannual variability. In Evans, G. T. and Fasham, M. J. R. (eds), *Towards a Model of Ocean Biogeochemical Processes*. Springer-Verlag, Berlin, pp. 237–260.

Thompson, J. M. T. and Stewart, H. B. (1986) *Nonlinear Dynamics and Chaos*. John Wiley and Sons, Chichester.

Truscott, J. E. (1994) Temporal and spatial behaviour of plankton ecosystems. PhD Thesis, University of Leeds, Leeds, UK.

Truscott, J. E. and Brindley, J. (1994) Equilibria, stability and excitability in a general class of plankton population models. *Philos. Trans. R. Soc. London Ser. A*, **347**, 703–718.

Wiggins, S. (1990) *Introduction to Applied Nonlinear Dynamical Systems and Chaos. Texts in Applied Mathematics. Vol. 2*. Springer-Verlag, New York.

Williams, R. (1988) Spatial heterogeneity and niche differentiation in oceanic zooplankton. In Boxshall, G. A. and Schimke, H. K. (eds), *Biology of Copepods. Hydrobiologia*, **167/168**, 151–159.

Yodzis, P. (1981) The stability of real ecosystems. *Nature*, **289**, 674–676.

Yodzis, P. (1988) The indeterminacy of ecological interactions as perceived through perturbation experiments. *Ecology*, **69**, 508–515.

Yool, A. (1998) The dynamics of open-ocean plankton ecosystem models. PhD Thesis, University of Warwick, UK; www.oikos.warwick.ac.uk/ecosystems/ThesisArchive.

Received on March 15, 2000; accepted on December 13, 2000

APPENDIX: CALCULATION OF STEADY STATES

A steady state, or equilibrium, of the system of equations (1)–(4) of Model 1 is a solution (N, P, Z, D) to $dN/dt = dP/dt = dZ/dt = dD/dt = 0$. Thus, a trajectory that starts from a steady state will simply remain fixed at the steady state, since none of the variables is increasing or decreasing in value. Whether a steady state is locally attracting or repelling depends upon the eigenvalues of the Jacobian matrix evaluated at that steady state. Edwards gives the detailed algebraic steps involved in calculating the steady states, plus the explicit Jacobian matrices and bifurcation diagrams (Edwards, 1997); here, we summarize those results.

The steady states of the system are obtained by solving the four simultaneous equations

$$0 = -\frac{N}{c+N} \frac{a}{b+cP} P + \frac{\beta \lambda P}{\mu+P} Z + \gamma d Z^m + \phi D + k(N_0 - N) \quad (11)$$

$$0 = \frac{N}{c+N} \frac{a}{b+cP} P - rP - \frac{\lambda P}{\mu+P} Z - (s+k)P \quad (12)$$

$$0 = \frac{c\lambda P}{\mu+P} Z - dZ^m \quad (13)$$

$$0 = rP + (1 - \alpha - \beta) \frac{\lambda P}{\mu+P} Z - (\phi + \psi + k)D \quad (14)$$

The simplest steady state is $(N, P, Z, D) = (N_0, 0, 0, 0)$; the nutrient concentration equals that in the deep water, and the mixed layer is devoid of life. The four eigenvalues of the Jacobian matrix are $-k, \Phi, 0$ and $-\phi - \psi - k$, where:

$$\Phi = \frac{aN}{b(c+N)} - r - s - k$$

The occurrence of a zero eigenvalue means that centre manifold analysis (Kuznetsov, 1995) would be required to deduce the stability of $(N_0, 0, 0, 0)$, but numerical simulations suggest that $(N_0, 0, 0, 0)$ is unstable for $\Phi > 0$ and stable for $\Phi < 0$. Essentially, if the phytoplankton growth rate is too low compared to the loss terms (r, s and k), then $\Phi < 0$ and the phytoplankton will die out, and consequently so will the zooplankton and detritus. This behaviour is directly analogous to the stability of the $(N, P, Z) = (N_0, 0, 0)$ steady state of the original NPZ model, and of NPZ models in general [e.g. (Busenberg *et al.*, 1990; Truscott and Brindley, 1994)].

Two more steady states are given by $(N_1^*, P_1^*, 0, D_1^*)$ and $(N_2^*, P_2^*, 0, D_2^*)$, where N_1^* and N_2^* are the two solutions to the quadratic equation

$$ckN^2 + \left[\frac{a(\Omega + s + k)}{c + s + k} - b(\Omega + s + k) + ck(c - N_0) \right] N - \left[b(\Omega + s + k) + ckN \right] c = 0 \quad (15)$$

where

$$\Omega = \frac{(\psi + k)r}{\phi + \psi + k}$$

and

$$P_1^* = \frac{k(N_0 - N_1^{**})}{\Omega + s + k} \quad (16)$$

$$D_1^* = \frac{r}{\phi + \psi + k} P_1^* \quad (17)$$

for $i = 1, 2$. The constant term of the quadratic (15) is negative, and so it has two real roots, one negative and one positive. We define N_1^* to be the positive root, and consider the ecologically unrealistic negative root N_2^* no further. We find that P_1^* has the same sign as Φ , and so as $\Phi \rightarrow 0$, we have $P_1^* \rightarrow 0, D_1^* \rightarrow 0$ and $N_1^* \rightarrow N_0$, i.e. $(N_1^*, P_1^*, 0, D_1^*) \rightarrow (N_0, 0, 0, 0)$. The steady state $(N_1^*, P_1^*, 0, D_1^*)$ is never stable (it has at least one unstable manifold), as was the case for the analogous steady state $(N_1^*, P_1^*, 0)$ for the NPZ model. However, if the $-dZ^2$ higher predation term is replaced by the linear form $-qZ$, then $(N_1^*, P_1^*, 0)$ can become stable (Edwards and Brindley, 1999). It is a consequence of the $-dZ^2$ mortality term [or any term $-dZ^m$ with $1 < m \leq 2$ (Edwards and Bees, 2001)] that the

zooplankton cannot die out if there are still phytoplankton available for grazing.

Finally, we find steady states of the form (N^*, P^*, Z^*, D^*) with non-zero values of all the variables. Such steady states are given by the solutions to

$$\zeta = \frac{\alpha\lambda P}{d(\mu + P)} \quad (18)$$

$$D = \frac{1}{(b + db + k)} \left[\epsilon P + \frac{(1 - \alpha - \beta)\alpha\lambda P}{d(\mu + P)} \right] \quad (19)$$

$$N = N_0 - \frac{(1 - \alpha\gamma - \beta)d\zeta}{k\alpha} + \frac{dbD}{k} - \frac{(s + k)P}{k} \quad (20)$$

[the right-hand side of equation (20) is in terms of P when equations (18) and (19) are substituted], and the values of P are the roots of a tenth-order polynomial in P . Writing the polynomial such that the coefficient of P^0 is one, the constant term of the polynomial is given by Ψ , where

$$\Psi = \frac{\frac{b\lambda\mu}{k}(\epsilon + N_0)(b + db + k)\Phi}{\epsilon[(s + k)(b + db + k) + \epsilon(db + k)](s + k)}$$

We see that Ψ is a positive multiple of Φ , and so $\Psi \rightarrow 0$ as $\Phi \rightarrow 0$, and at $\Phi = 0$, $P = 0$ becomes a solution of the tenth-order polynomial. An (N^*, P^*, Z^*, D^*) solution thus degenerates to $(N_0, 0, 0, 0)$ at $\Phi = 0$, suggesting that we have a ‘three-way transcritical bifurcation’ (Truscott, 1994); this bifurcation is shown graphically by Edwards and Bees for the NPZ model (Edwards and Bees, 2001). At such a bifurcation, the steady states $(N_1^*, P_1^*, 0, D_1^*)$ and (N^*, P^*, Z^*, D^*) are both equal to $(N_0, 0, 0, 0)$. Setting all of the parameters to their default values given in Table I, upon solving the aforementioned tenth-order polynomial and using equations (18), (19) and (20), we find only one solution of the form (N^*, P^*, Z^*, D^*) with strictly positive values of all of the variables. Therefore, if all parameters are set to their default values, and a numerically computed trajectory is attracted to a steady state with $N, P, Z, D > 0$, as in Figure 2a, then we know that this is the unique steady state with strictly positive values of all four variables. However, we find that multiple steady states are possible when parameters are varied from their default values (Figure 4). Analytical calculation of the stability of (N^*, P^*, Z^*, D^*) is unfeasible.

The steady states for Model 2 are obtained by solving the four simultaneous equations

$$0 = -\frac{N}{\epsilon + N} \frac{\alpha}{b + \epsilon P} P + \frac{\beta\lambda(P + \omega D)\zeta}{\mu + P + \omega D} + \gamma d\zeta + dbD + k(N_0 - N) \quad (21)$$

$$0 = \frac{N}{\epsilon + N} \frac{\alpha}{b + \epsilon P} P - rP - \frac{\lambda P Z}{\mu + P + \omega D} - (s + k)P \quad (22)$$

$$0 = \frac{\alpha\lambda(P + \omega D)\zeta}{\mu + P + \omega D} - dZ \quad (23)$$

$$0 = \epsilon P + \frac{[(1 - \alpha - \beta)P - (\alpha + \beta)\omega D]\lambda\zeta}{\mu + P + \omega D} - (b + db + k)D \quad (24)$$

Clearly, solutions which have $Z = 0$ will have the same definitions as those for Model 1, since the new grazing functions (the only difference between the models) always appear as a multiple of Z . So there is a steady state $(N_0, 0, 0, 0)$, which numerical simulations again suggest is unstable for $\Phi > 0$ and stable for $\Phi < 0$. As for Model 1, the steady state $(N_1^*, P_1^*, 0, D_1^*) \rightarrow (N_0, 0, 0, 0)$ as $\Phi \rightarrow 0$, and $(N_1^*, P_1^*, 0, D_1^*)$ is never stable.

For Model 1, the dZ/dt equation only contains P and Z , and is independent of N and D . This means that $dZ/dt = 0$ can be rearranged to express Z in terms of P in order to calculate steady states with $Z \neq 0$, as given by equation (18). However, D appears explicitly in the dZ/dt equation of Model 2. So, from equation (23), we cannot express Z in terms of P alone, but as a function of P and D , namely:

$$\zeta = \frac{\alpha\lambda(P + \omega D)}{d(\mu + P + \omega D)} \quad (25)$$

Adding equations (21), (22), (23) and (24) gives, upon rearrangement, the following expression for N :

$$N = N_0 - \frac{(1 - \gamma)d\zeta}{k} - \frac{(s + k)P}{k} - \frac{(b + k)D}{k} \quad (26)$$

Thus we can express N and Z in terms of P and D . When we substitute for N and Z into equations (21) and (24), we obtain a pair of multivariate polynomials in P and D . One polynomial is sixth order, and the other is eleventh order, making any further analysis impossible. This is unlike Model 1, for which, although we could only reduce the solutions to a single tenth-order polynomial in P , we could show that the constant term of the polynomial tends to zero as $\Phi \rightarrow 0$ and so the (N^*, P^*, Z^*, D^*) solution degenerates to $(N_0, 0, 0, 0)$ at $\Phi = 0$, which is the three-way transcritical bifurcation. However, numerical computations show that the three-way transcritical bifurcation does occur for Model 2, and so (N^*, P^*, Z^*, D^*) exchanges stability with $(N_0, 0, 0, 0)$ at $\Phi = 0$.